Polyhedron 155 (2018) 232–253

Contents lists available at ScienceDirect

Polyhedron

journal homepage: www.elsevier.com/locate/poly

The insights from X-ray absorption spectroscopy into the local atomic structure and chemical bonding of Metal–organic frameworks

Mikhail A. Soldatov [a,*], Andrea Martini [a,b], Aram L. Bugaev [a], Ilia Pankin [a,b], Pavel V. Medvedev [a], Alexander A. Guda [a], Abdelaziz M. Aboraia [a,d], Yulia S. Podkovyrina [a], Andriy P. Budnyk [a], Alexander A. Soldatov [a], Carlo Lamberti [a,c]

[a] The Smart Materials Research Institute, Southern Federal University, Sladkova str. 178/24, Rostov-on-Don, Russia
[b] Department of Chemistry and NIS Centre, University of Turin, via P. Giuria 7, Turin, Italy
[c] Department of Physics, CrisDi and NIS Interdepartmental Centres and INSTM Reference Center, University of Turin, via Pietro Giuria 1, 10125 Turin, Italy
[d] Department of Physics, Faculty of Science, Al-Azhar University, Assiut 71542, Egypt

ARTICLE INFO

Article history:
Received 25 June 2018
Accepted 4 August 2018
Available online 14 August 2018

Keywords:
MOFs
XAS
EXAFS
XANES
Operando

ABSTRACT

After a short introduction highlighting the potentialities of metal–organic frameworks (MOFs) and the power of X-ray absorption spectroscopies (XAS), a list of selected examples follows. The first part of this review provides the basic concepts that are behind the most used XAS techniques: Extended X-ray Absorption Fine Structure (EXAFS) and X-ray Absorption Near Edge Structure (XANES) spectroscopies. Moreover, it reports also the basis of an innovative approach to the EXAFS data analysis based on the wavelet transform approach, that allows a more solid attribution to the different paths contributing to the overall signal. The second part is devoted to provide a section of examples where EXAFS and XANES techniques have been determinant in understanding the structural and electronic properties of metal centers in MOFs. The selected examples have been ordered in subsections related to the application foreseen for the investigated MOFs materials: MOFs functionalization for catalytic applications; MOFs as single site catalyst; MOFs as photocatalysts; MOFs for gas sorption and storage; MOFs for energy application. Conclusions and perspectives are provided at the end.

1. Introduction

The role of zeolites as leading class of crystalline porous materials has been challenged in the last twenty years by metal–organic frameworks (MOFs), also known as coordination polymers [1–21]. Although the industrial application of MOFs is still limited to few cases [22,23], this new class of materials is foreseen to play an important role in the next future, in the fields of gas separation and purification [24,25], liquid phase separation [26–28], gas storage [29–44], sorption of toxic or radioactive metal ions [45–51], drug delivery [52–62], chemical sensors [63–65], optical materials [63,65–80], magnetic materials [81–88], solid state ion conductors [89–92], electrochemical energy storage [93,94], semiconductors [95–99], electronic and optoelectronic [65,100–102], supercapacitor [103–106] or low-κ dielectric materials [107,108], catalysis [109–120], electrocatalysis [94,121–126], photocatalysis [127–137] and biocatalysis [138–144]. Moreover, some MOFs are able to respond to external stimuli (such as pressure, temperature, and adsorption of guest molecules) with interesting reversible framework modifications [145].

MOFs diverge from zeolites in important ways [2,3]. The most important one being their larger diversity and tunability in composition and less topological constraints in the formation of the porous lattices. The enormous number of new MOF frameworks reported every year reflects this flexibility and the large interest for their potential applications [146]. Zeolites are restricted to tetrahedral networks, the inorganic cornerstone in MOF topologies may be a single metal atom or a more or less complex cluster of

Abbreviations: DOS, density of states; EXAFS, extended X-ray absorption fine structure; FT, Fourier transform; MIL, materials of Institute Lavoisier; MOF, metal–organic framework; RIXS, resonant Inelastic X-ray scattering; RMS, root mean square; UiO, Universitetet i Oslo (University of Oslo); UPS, ultraviolet photoelectron spectroscopy; WT, wavelet transform; XAFS, X-ray absorption fine structure; XANES, X-ray absorption near edge structure; XAS, X-ray absorption spectroscopy; XES, X-ray emission spectroscopy; XFEL, X-ray free electron lasers; XPS, X-ray photoelectron spectroscopy; XRD, X-ray diffraction.

* Corresponding author.
E-mail address: mikhail.soldatov@gmail.com (M.A. Soldatov).

https://doi.org/10.1016/j.poly.2018.08.004
0277-5387/

coordinated metal atoms or extended inorganic sub structures extending in one, two or three dimensions.

Such an enormous framework flexibility and variation in structural motifs [12,14] represents also a challenge in the characterization of MOF materials. Most structures have been solved from single crystal data. In the few cases where this approach is practicable, the structure can be retrieved ab initio, although care is needed because the huge cell volume and the high number of atoms in the unit cell (typical of MOFs) may induce some pitfalls in the structure solving process [147]. In all other cases, when only powder XRD (XRPD) data are available additional structural information, particularly regarding local coordination within the inorganic cluster, are often mandatory in order to solve the structure [148–151]. There are also cases were the inorganic cluster does not follow the symmetry of the overall structure [45,152–154]. In such cases diffraction techniques will just "see" an average structure, missing the local structure: a lack that may be critical for understanding the specific properties to the material. In both cases, extended X-ray absorption fine structure (EXAFS) spectroscopy [155–163], taking benefit from its atomic selectivity, is the tool that will give us this complementary structural information on the inorganic cluster and the way it binds to the ligand [164–166]. The fact that MOFs are mainly constituted by low Z elements (C, O, N, H), that are almost transparent to X-rays, allows to collect, at the metal K- or L-edges, high quality transmission X-ray absorption spectra characterized by an optimized edge jump $\Delta\mu x$ as high as 1.0–1.5, resulting in accurate data, analyzable up to 15–18 $Å^{-1}$ [148,149,167-169], vide infra Fig. 7a. The complementarity between long range order, investigated by diffraction techniques, and local range order, investigated by EXAFS, has already been recognized for complex systems, such as metalloproteins [170–183], disordered mixed metal-oxides [184–186] ternary and quaternary semiconductor solid solutions [187–194] and MOFs [164–166]. On the other hand, also the region near the edge of the X-ray absorption spectrum, X-ray absorption near edge structure (XANES) [195–199], has made in the last decade remarkable improvements in its ability to provide quantitative structural and electronic properties of the selected element [200–204].

Besides this brief introduction, this review is divided into two main parts. The first one (Section 2) devoted to describe the XAFS methods and the second (Section 3) devoted to provide relevant examples of the use of XAFS spectroscopies in the characterization of MOFs. Finally, Section 4 provides conclusions and new perspectives.

2. Methods

In this section, we will provide the basic general concepts of XANES and EXAFS spectroscopies (Section 2.1) and of a more advanced way to interpret EXAFS spectra looking in both k- and R-spaces, that is the wavelet transform method (Section 2.2).

2.1. X-ray absorption spectroscopy: general aspects

X-ray absorption spectroscopy [155–161,163] is the ideal technique to investigate the structural and electronic configuration of metal centers hosted inside nanostructured materials such as MOFs [164,166]. Such methods investigates the fine structure of X-ray absorption (the international term is X-ray Absorption Fine Structure – XAFS spectroscopy or XAS – X-ray Absorption Spectroscopy) that is present across a specific edge (K, L, M) of a selected element [205,206]. Unlike X-ray scattering techniques, XAS is consequently an element selective technique. XAS experiments are mainly performed at large scale research facilities (synchrotron radiation sources) able to provide a brilliant X-ray source in a very large energy interval from soft to hard X-rays (although also IR, visible and UV regions are covered) [207]. The high flux and the high brilliance of the X-ray beams generated at synchrotron sources makes time [208–210] and space [211,212] resolved experiments possible. The high flux allows also highly diluted samples to be measured, while focused beams [211,212] allows the measurements on samples where only a small amount of a substance is available, such as in the fields of high pressure physics [213], cultural heritage [214] and radioactive materials [215]. Measurements of the X-ray absorption spectrum can be carried out in several ways [194]. The "true" X-ray absorption is measured by determining the ratio in the X-ray intensity before and after the sample (Fig. 1a). However, such a direct method of measurement is not always possible to realize, since it makes high demands on the homogeneity and thickness of the sample being studied. Moreover, it cannot be applied if the selected element is too diluted in the sample matrix. In such cases, alternative methods, based on the measurement of secondary processes, can be applied. Indeed, the primary process (that is the creation of the core hole in the K, L or M edge of the selected element due to the photoelectric effect) is followed by deexcitation process where the core hole is filled by a higher shell electron with the emission of either an X-ray fluorescence photon or and Auger electron. As a consequence, the measure of the X-ray fluorescence yield (Fig. 1b), or of the total or partial electron yields emitted by the sample (Fig. 1c), provides a response that is proportional to the primary process.

The choice of specific detection method among those described in Fig. 1 is determined by the characteristics of the samples being studied and the specific tasks of the study [205,216]. Samples can be in any aggregate state [216,217]. Although experimentally acquired in the same data collection, the XAFS spectrum is traditionally divided into two main parts: the region of the near (XANES) and far away (EXAFS) from the adsorption edge (Fig. 2).

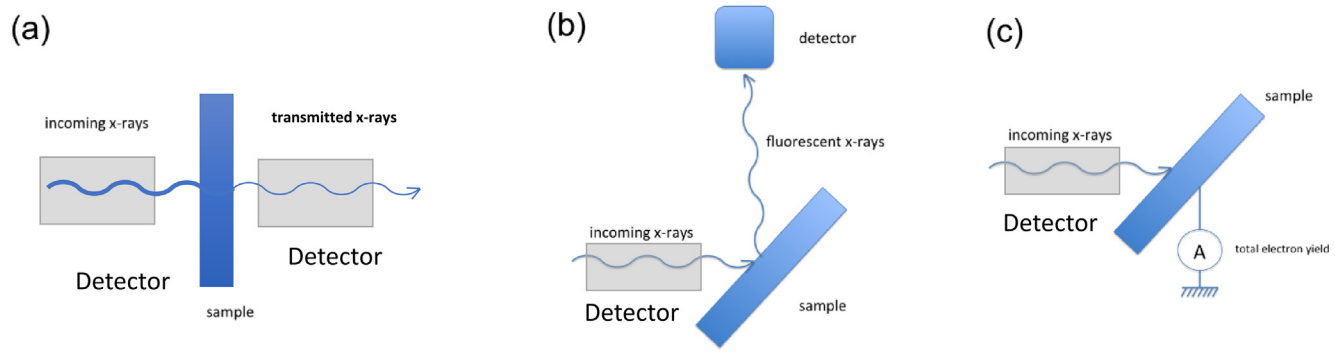

Fig. 1. The scheme of the experiment for detection by several methods: true absorption – "transmission" (a), fluorescence yield (b), total electron yield (c).

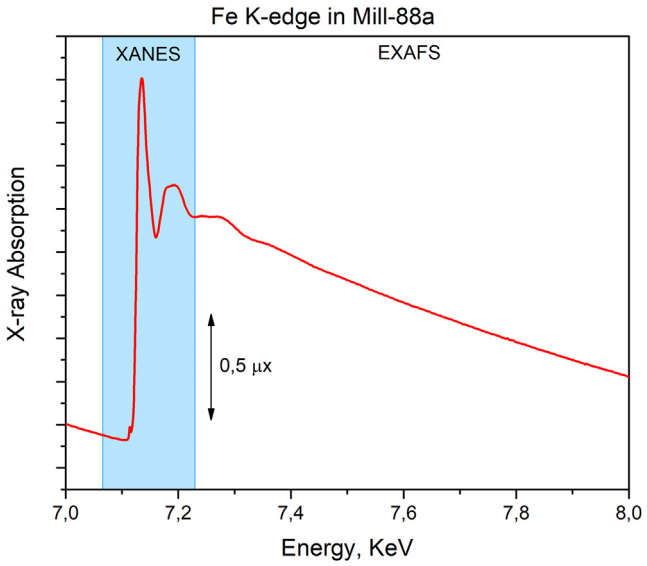

Fig. 2. Full Fe K-edge X-ray absorption spectrum of MOF MIL-88a including both XANES and EXAFS regions.

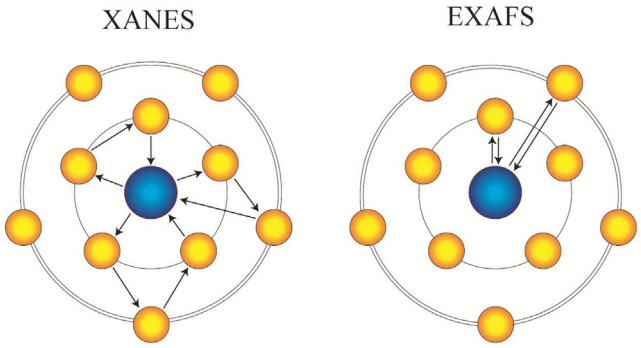

Fig. 3. Multiple scattering responsible for XANES and single scattering path for EXAFS.

Although XANES and EXAFS are of close origin, they are treated in different ways, since the information that can be obtained from these two parts of the XAFS signal differs significantly [158,159,218,219]. Analysis of XAFS spectra allows to obtain the information on the position of atoms in the vicinity of several coordination spheres near the X-ray exciting atom, including bond lengths and bond angles.

EXAFS is successfully used to analyze such a parameter of local atomic structure like radial distribution of atoms around the selected element in materials without long range order [162,220,221] and liquids [222]. The objects of choice are ultra small nanoclusters [223–227], quantum wells [188-191,193,228], quantum dots [229–233], thin films (down to few monolayers) [192,228,234–237], active metal sites in metalloproteins [170–183] and crystals with impurity defects [238]. The way of analysis of the X-ray absorption coefficient in the EXAFS spectral region extending from about 30 eV above the edge is more direct compared to the XANES spectral region that extends from the absorption edge up to about 100 eV above the edge [198,199].

The change in the symmetry of local environment of the atom (the angles of the chemical bond) [239–242], even without changing the distance between the absorbing atom and its neighbors and the number of neighbors, leads to visible changes of the XANES shape, while the EXAFS shape remains unchanged [182] (this holds when multiple scattering paths can be neglected in the EXAFS analysis). This is explained by the shorter mean free path of the photoelectron at energies corresponding to the region of EXAFS, which limits the EXAFS signal origin mostly to single scattering processes of the photoelectron wave by the surrounding atoms (see Fig. 3) [218]. This makes the EXAFS spectra a rather direct tool to obtain information on such important structural parameters as bond lengths and coordination numbers [155]. EXAFS spectroscopy can be sensitive to local geometry and bond angles, in case multiple scattering paths are relevant in the overall signal [156,157,243-247]. Multiple scattering paths are particularly strong in case of collinearity among there or more atoms such as in solids with rock salt [234,237,248] or fcc [249-251] structures or in metal-carbonyl [200,252–257] or metal-nitrate [258] complexes.

Besides these peculiar exceptions (and few similar ones) XANES spectroscopy, which includes a near-edge region up to about 100 eV behind the edge, is much more sensitive than EXAFS one to bond angles and local geometry around the X-ray absorbing atom [202], in addition to the sensitivity on oxidation states [184,204,259–265] and bond lengths [266–270]. Thus, with XANES analysis one could study not only local atomic structure parameters, but electronic structure as well. By the analysis of main X-ray absorption edge energy shift it is possible to determine the oxidation state of the ion (atom) under study. Moreover, as the XANES is proportional to the corresponding projected density of unoccupied density of electron states (DOS) [271], one could estimate this important function, which determines many physical and chemical properties of the material [272].

However, the determination of a complete three-dimensional local atomic structure of a material without long-range order in the arrangement of atoms requires advanced theoretical analysis of XANES data [273] and includes time-consuming *ab-initio* theoretical simulations of XANES spectra using based on different approaches. There is a number of codes based on DFT/TDDFT and many-body approximations. The most popular Green function method is available in the programs FEFF [198,274,275], CONTINUUM [276,277], FDMNES [199,202,278,279], SPRKKR [280,281], MXAN [195,196,282], and XKDQ [283,284]. Most of it is based on multiple scattering theory that uses muffin tin approximation. However, the finite difference approximation offers an efficient and accurate way of modeling metal–organic frameworks active centers using full potential that is most accurate for systems with string covalent bonds and large voids [202,278]. There are also codes based on basis set approach such as ADF [285], ORCA [286,287], Gaussian, Wien2k [288–290], Quantum Espresso [291–293] and PARATECH [294]. Many-body approximation is usually used for 3d transitional metals $L_{2,3}$ edge and the pre-edge area of K-edge spectra and includes such approaches as atomic multiplets implemented in QUANTY [295], XTLS [296], and CTM4XAS [297]; Bethe-Salpeter equation used in OCEAN [298,299], EXC!TiNG [300,301]; post Hartree-Fock approach used in MOLCAS [302]. Usually powerful supercomputers or cloud computing [303,304] are needed to determination of a complete three-dimensional local atomic structure. It should also be stressed that there is no direct route for determination of the 3D local atomic structure parameters from XANES. Possible approaches proposed are based on the fitting of theoretical XANES simulated for "probe" models of local atomic structure for the materials under study to the experimentally obtained XANES [197,305,306].

MXAN code is based on the comparison between the experimental spectrum and several theoretical calculations performed by changing selected structural parameters from a starting putative structure, i.e. from an initial configuration of the atoms around the absorber [195-197]. The MXAN package makes use of the CONTINUUM code [305] to calculate the absorbing cross section in the framework of the full MS approach, i.e. the scattering path operator

is calculated exactly, without any series expansion. The calculated spectra are then convoluted with a Lorentzian function of constant width to mimic the spectral broadening due to the core–hole lifetime and the experimental resolution. The basic idea implemented in FitIt code [273,307], which is the variation of structural parameters and minimization of the discrepancy between theory and experiment, is the same as in MXAN. The difference between them is that MXAN is linked to only one implementation of the full multiple scattering approach, it does not use the multidimensional interpolation and therefore does not provide the same possibilities for visualization and combination with more precise, but computationally time-consuming methods. Within FitIt approach [273,307] the XANES fitting includes two steps: interpolation of XANES spectra and minimization of discrepancy between theory and experiment. First, one should construct the interpolation of the spectrum as a function of structural parameters. It allows the prediction of XANES for any values of parameters within the selected limits of variation. A second step is a minimization of the discrepancy between interpolated and experimental XANES spectra by varying the structural parameters. Thus, one obtains the "best-fit" set of the local atomic structure parameters (i.e. the most probable 3D local atomic structure of the material under the study) spending reasonable computer resources. At a later stage, to deal with the growing number of XANES spectra measured in the processes having simultaneously several phases, the principal component analysis (PCA) option is also included [306].

Finally, one should mention that if possible it is better to use both XANES and EXAFS methods to study thoroughly the local atomic and electronic structures of the nanostructured materials in a self-consistent way [308,309].

2.2. Wavelet transform applied in the analysis of EXAFS spectra

The EXAFS signal, usually defined as the $\chi(k)$ function, is characterized by weak oscillatory wiggles of the X-ray absorption coefficient that arise from the interference between the parts of the photoelectron wavefunction diffused from the absorber atom and backscattered by its neighbours [155,157–161,163]. As described by Sayers, Lytle and Stern in their milestone works [220,310,311], background subtracted EXAFS oscillations can be related *via* Fourier Transform (FT) to a specific spatial arrangement (in R-space) of atoms groups located around of the absorber.

In the single scattering approximation, the theoretical relation between the modulation of the EXAFS signal $\chi(k)$ (where k is the photoelectron wave-vector) and the structural parameters can be expressed by the following equation [155,158]:

$$\chi(k) = S_0^2 \sum_i \frac{N_i}{R_i^2} \frac{F_i(k,R)}{k} e^{-\frac{2R_i}{\lambda(k)}} e^{-2\sigma_i^2 k^2} \sin(2kR_i + \phi(k,R)) \quad (1)$$

where the summation is performed over each shell of neighbouring atoms i. In this formula, the parameter R_i indicates the interatomic distances of the i^{th} shell from the absorber. S_0^2 is the overall amplitude reduction factor [312], $F_i(k,R)$ is the electron backscattering amplitude, N_i is the coordination number (number of equivalent scatterers), σ_i is the Debye–Waller factor which accounts for the thermal and static disorder while $\lambda(k)$ represents the energy-dependent electron mean free path. The terms $\phi(k,R) = \delta(k) + \theta_i(k,R)$ describes the total phase shift due to the presence of central (δ) and backscattering atoms of the i-th shell (θ_i as reported in Fig. 4b) and plays a fundamental role in the FT-peaks positioning.

One limit of the EXAFS spectral analysis, based on FT, can be found in the impossibility to identify group of different atoms located at close distances. In this case, their contributions in R-space overlap, making their discrimination difficult to realize. However, Teo and Lee [155,313] calculations demonstrated the dependence of $F_i(k,R)$ and $\phi(k,R)$ with the atomic number Z in the EXAFS range. In particular, for low Z atoms $F_i(k,R)$ becomes larger at low k values and decreases almost monotonically with k (Fig. 4a). As Z increase a maximum appears at larger k values. For highest Z atoms two maxima become evident [155,315]. The characteristic behavior of both $\phi(k,R)$ and $F_i(k,R)$ as a function of Z can be used to distinguish type of scattering atoms if their atomic numbers are sufficiently different [165]. In fact, their contributions are localized at different k-ranges.

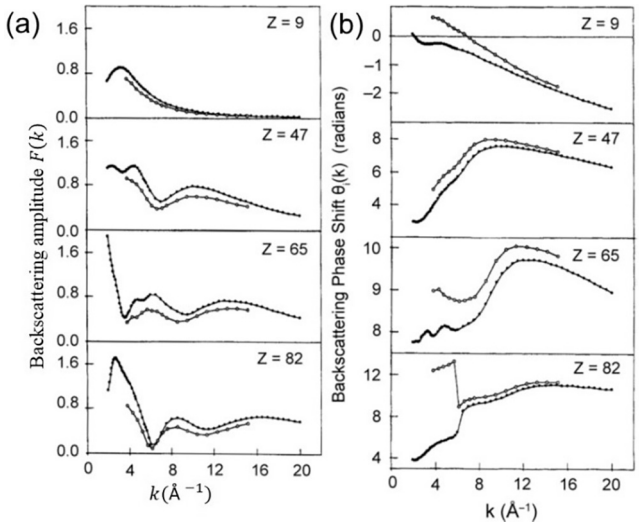

Fig. 4. Backscattering amplitude (a) and phase shift (b) as a function of k for different elements: F ($Z = 9$), Ag ($Z = 47$), Tb ($Z = 65$) and Pb ($Z = 82$). Open and full circles refer to the work of Teo et al. [313] and McKale et al. [314] respectively. Adopted with permission from Ref. [313] and [314]. Copyright 1979, 1988 American Chemical Society.

In this context Wavelet Transform (WT) analysis can be employed with great advantages in the analysis of the EXAFS spectra [316–321]. In the field of XAS spectroscopy, wavelet analysis was initially used for EXAFS background subtraction [316] and to reconstruct the radial distribution function from noisy EXAFS spectra [317]. However, the power of this technique principally stands in the possibility to obtain a 2D correlation plot of the EXAFS signal with its simultaneous localization in R and k space [318–321]. In this way, it is possible to reduce the ambiguities related to the identification of backscattering atoms which come from the FT-analysis.

Formally, the WT of a given k^n-weighted EXAFS spectrum is expressed as:

$$w(a,b) = \frac{1}{\sqrt{a}} \int_{-\infty}^{+\infty} dk' k'^n \chi(k') \psi^* \left(\frac{k'-b}{a} \right) \quad (2)$$

This equation can be seen as the inner product between the analysed spectrum $\chi(k)$ and a defined window function ψ, called "mother wavelet" or simply wavelet (where the apex ψ^* denotes the complex conjugate of ψ), that must satisfy following the zero-mean condition:

$$\int_{-\infty}^{+\infty} dk' \psi(k') = 0 \quad (3)$$

Differently from the FT, where a signal is decomposed into a linear combination of sine and cosine waves at different frequencies, in the WT approach the signal $\chi(k)$ is analysed through a set of train-waves (wavelets) that are shifted by b units in the k-space and distorted by a factor a in order to keep account of the local frequencies of the signal. The variables a and b are connected to the k and R-space by the following relations [318,320]:

$$b = k$$

$$a = \frac{\eta}{2R} \tag{4}$$

where η is a parameter related to the typology of the wavelet used. Its meaning will be discussed below. From Eq. (4) the expression of the WT finally becomes:

$$w(R,k) = \sqrt{\frac{2R}{\eta}} \int_{-\infty}^{+\infty} dk' k'^{n} \chi(k') \psi^{*} \left[\frac{2R}{\eta}(k' - k)\right] \tag{5}$$

The local resolution in the reciprocal Δk and direct space ΔR are stated in terms of Root Mean Square (RMS) values [322], generating k-R windows (or uncertainty cells) of constant area where the signal information is distributed:

$$[k \pm \Delta k] \times [R \pm \Delta R] = \left[k \pm \frac{\eta}{2R}\Delta k_{\psi}\right] \times \left[R \pm \frac{2R}{\eta}\Delta R_{\psi}\right] \tag{6}$$

where Δk_{ψ} and ΔR_{ψ} are the RMS of the chosen wavelet in k and R space respectively [323]. This means that if two signal contributes differ in k space of a quantity lower than $2\Delta k$ or have a frequency (i.e. $\pi\omega = R$) smaller than $2\Delta R$, they cannot be resolved [321].

For the EXAFS data analysis, two kind mother wavelets are used. The first one is the Morlet wavelet [319–321] that is composed by a fast oscillatory part confined by a Gaussian envelope making its real and imaginary part similar to an EXAFS spectrum:

$$\psi_{\eta,\sigma}(k) = \frac{1}{\sqrt{2\pi\sigma}} e^{i\eta k} e^{-k^2/2\sigma^2} \tag{7}$$

where η, introduced in Eq. (4), represents the frequency of sine and cosine waves while σ corresponds to the Gaussian standard deviation. These two parameters must be chosen accurately because they play a critical role in the optimization of the WT resolution. In fact, η and σ appear together in the analytical expressions of Δk_{ψ} and ΔR_{ψ}, which are constrained by the Heisenberg inequality: $\Delta k_{\psi} \Delta R_{\psi} \geq 1/2$ [322]. Considering expression (7), its related uncertainly cell is given by:

$$\left[k \pm \frac{\eta\sigma}{\sqrt{2}R}\right] \times \left[R \pm \frac{R}{\sqrt{2}\eta\sigma}\right] \tag{8}$$

Hence the k-R window is narrowed in the k space for large values of R while it becomes wider for small R. Reciprocally, the resolution in R space decrease by increasing R [320].

The second mother function commonly used in the EXAFS signal analysis is the Cauchy wavelet. It has been introduced by Muñoz et al. [318] and it is defined as:

$$\psi_{\eta}(k) = \left(\frac{i}{k+i}\right)^{\eta+1} \tag{9}$$

where i is the imaginary unit while η is the so-called "Cauchy parameter". Its related uncertainly cell is:

$$\left[k \pm \frac{1}{R}\left(\frac{\eta}{2\sqrt{2\eta - 1}}\right)\right] \times \left[R - \frac{1}{R}\left(\frac{1}{2\eta} - \frac{\sqrt{2\eta-1}}{2\eta}\right), R + \frac{1}{R}\left(\frac{1}{2\eta} + \frac{\sqrt{2\eta-1}}{2\eta}\right)\right] \tag{10}$$

Analysing expression (10) it is evident that the window shape in the R-space is asymmetric and the resolution is controlled by just one parameter: η. However, same observations discussed for the Morlet k-R window remain valid. The choice of the Cauchy wavelet must be found in the possibility to simplify the integral of Eq. (2), moreover the use of a complex-valued function is well suitable for analyzing frequency-modulated signals [318].

Fig. 5 reports two examples where WT is applied in the analysis of two model signals $\chi_1(k)$ and $\chi_2(k)$ (Fig. 5a,d) and related FT (Fig. 5b,e):

$$\chi_1(k) = 2sin(4k)e^{-(k-3)^2} + sin(8k)e^{-(k-7)^2}$$

$$\chi_2(k) = 2sin(4k)e^{-(k-5)^2} + sin[6k(1+0.1k)]e^{-\frac{1}{2}(k-10)^2} \tag{11}$$

Both signals $\chi_1(k)$ and $\chi_2(k)$ are composed by the sum of two periodic functions localised in a range of k values by two Gaussians with different centers. As it is possible to see from both Fig. 5b the discrimination of the two contributes from the FT-moduli analysis is not straightforward. However, as described before, WT keeps also account of the signal "localization" in k-space making the distinction of the two contributions easier to realize in the 2D plot, as reported in Fig. 5c. Note that signal χ_2 differs from signal χ_1 principally for the presence of a non-linear (quadratic) phase term that is responsible of the lobe inclination in the corresponding WT-magnitude plot Fig. 5f. In this case FT provides directly a scenario where the shell peaks are well resolved in the R-space. However, the wavelet-tilting phenomenon, that in the time–frequency language is called "chirp" [319], can be used to point out the presence of heavier elements in a chemical compound, which are characterized by sharp (non-linear) changes in $\phi(k,R)$.

3. Local atomic structure and chemical bonding of metal–organic frameworks investigated by XAFS techniques.

3.1. Designing new efficient catalysts by MOFs functionalization

The exceptional porosity and high specific surface area of MOFs make them attractive candidates for catalytic applications [23,112,114,115]. However, only few of MOF types exhibit catalytic activity themselves, as the metals in the inorganic cornerstones

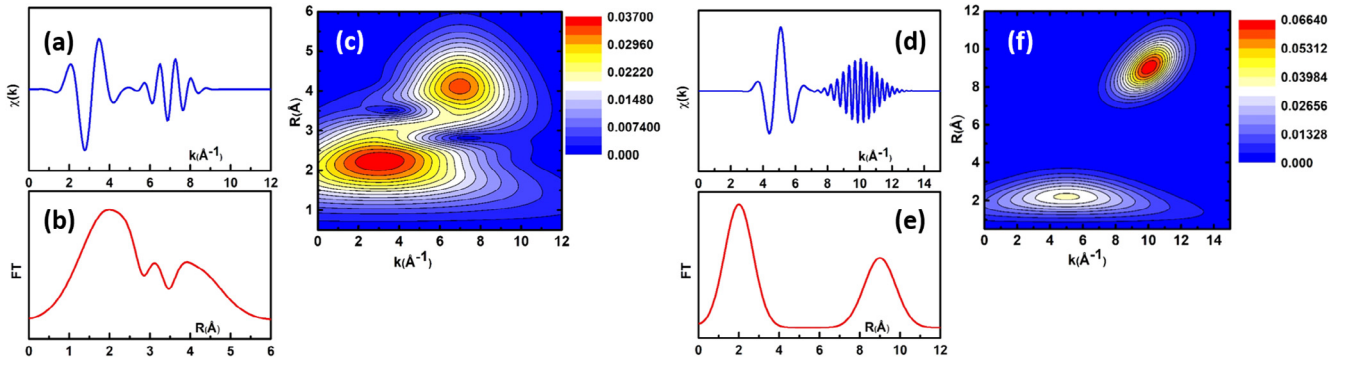

Fig. 5. (a) Model signal χ_1, (b) modulus of its Fourier transform, (c) modulus of its Cauchy WT. (d) Model signal χ_2, (e) modulus of its Fourier transform, (f) modulus of its Cauchy WT. For both signals it has been used a Cauchy parameter η fixed to 200.

normally do not possess coordination vacancies, except some that have only one coordination vacancy (e.g. CPO-27-M [167–169,33,324,325]). To provide additional functionalities to MOFs, various functionalization methods have been proposed [326–332]. Particularly, interesting for catalytic activities are the MOFs of the UiO-66, -67 and -68 family, because of their exceptional thermal stability and their resistance in acidic media [152–154]. For UiO-67 framework [154], functionalization can be made via incorporation of metal ions into the structure of the linker (see Fig. 6). The further activation of such material may result either in removal of ligands and formation of isolated active metal ions, or in reduction of metals and formation of metal nanoparticles inside the pores of MOF. Such approach have been successfully applied for incorporation of iron [333], nickel [334], copper [335–337], ruthenium [127], rhodium [338,339], iridium [127,339], rhenium [127], platinum [337,340–343], and palladium [344–346]. Investigation of the local structure around the active metal sites in functionalized MOFs is a typical problem where element-selective X-ray absorption spectroscopic methods can provide the most detailed information.

The recent study by Bugaev et al. [346] demonstrates an example of a combined *operando* XANES/EXAFS/XRD investigation to reveal the evolution of Pd species in Pd-functionalized UiO-67 MOF (Fig. 7). As only 5–10% of the standard bpdc linkers can be functionalized with ($PdCl_2$)bpydc, the incorporated metal ions are normally below the detection limit of XRD methods. In this case, EXAFS spectroscopy measured on a sample of optimal thickness allows observation of two distinguished coordination shells at 2.03 and 2.29 Å, corresponding to Pd–N and Pd–Cl contributions. Activation of the material in hydrogen leads to reduction of Pd^{II} to Pd^0 with formation of palladium nanoparticles mainly hosted inside the pores of the UiO-67 MOF. The reduction process is best observed in the XANES region, while observation of Pd–Pd peak in the Fourier-transformed EXAFS data confirms the nanoparticle formation. Also in the latter case, XRD data fail to detect the Pd particles, due to their small concentration and nanometric size.

The resulting material has been tested for the model reaction of ethylene hydrogenation and demonstrated high catalytic activity. The interaction of ethylene molecules with palladium nanoparticles was evidenced by the characteristic XANES features of palladium carbide [308,309,347], which proved the accessibility of the palladium nanoparticles by the molecules of the reagent.

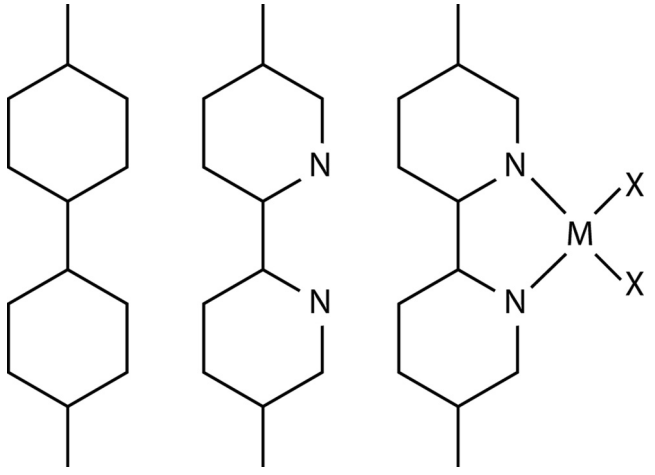

Fig. 6. Carton showing the functionalization of UiO-67 via the use of modified linkers hosting the metal M with ligand X. Left: standard bpdc linker; middle: modified bpydc linker; right: functionalized (MX_n)bpydc linker (M = Fe, Ni, Cu, Ru, Rh, Re, Pd, Pt; X = Cl, Br, n = 2,3,4).

Interestingly, the Pt-functionalized UiO-67 MOF was investigated by combining EXAFS and XANES analysis, revealing the formation of isolated Pt-ions and Pd nanoparticles, depending on the activation conditions [336,337,340,343].

Summarizing, together with a number of other examples, these studies clearly demonstrate the fundamental role of X-ray absorption spectroscopy in characterization of active metal species and investigation of the structure–reactivity relationships in the functionalized MOFs.

3.2. MOFs as single site catalysts for energy applications

Energy generation shifts to a renewable sources and a research focus moves to new electrochemical materials for energy conversion. The most important reactions such as oxygen reduction reaction (ORR), oxygen evolution reaction (OER), and hydrogen evolution reaction (HER) are catalyzed by such materials. That is why single atom catalyst on amorphous carbon-based materials derived from MOFs recently attract amount of attention for their applications in energy and catalytic field, such as ORR [348,349], HER [350,351], OER [352], etc [353]. One of the most promising applications for WT-EXAFS analysis (see Section 2.2) are single site catalysts, as its catalytically active sites consists in isolated ions or a very small group of metallic atoms which are usually incorporated into framework materials or deposed on the substrate [354–360]. In some cases, conventional XAS-analysis usually encounters the problem of segregation of the signal originated by the framework and extra-framework species. The next few paragraphs are aimed to emphasize possible application of WT-EXAFS analysis on MOFs.

As described in detail in Section 2.2, in contrast to the commonly used FT approach, the WT provides information regarding the localization of different EXAFS signal components in both k- and R-spaces simultaneously [361]. This approach affords superior discrimination of EXAFS contributions from different species, as the phase and backscattering amplitude from different elements are emphasized in different regions of k-space [319,321,362]. Thereby multiple scattering paths from light elements, which possess the same half-path length as direct scattering paths from heavier elements, can be readily deconvoluted through simple inspection of the WT [321]. This makes wavelet analysis a powerful tool for all cases in which it is important to discriminate contributions from the different elements, located about the same distance to the absorbing atom.

Automatically dispersed catalysts comprising mononuclear metal complexes or single metal atoms on supports offer maximum atom efficiency and provide the most ideal strategy to create highly efficient catalysts [363,364]. Moreover, catalysts with atomically dispersed active sites are model systems that allow understanding of heterogeneous catalysis at the molecular level, bridging the gap between heterogeneous and homogeneous catalysis [365].

An efficient way for carbon dioxide reduction by using of single atom implemented MOF described by Zhang et al. [365]. The newly developed MOF-525-Co is able to selective capture and photo reduce CO_2 with high efficiency under visible-light irradiation (so called "visible-light-driven carbon dioxide photoreduction"). Low charge separation and energy transfer efficiency, as well as inconsistencies between catalytic and adsorption sites, are main drawbacks to visible-light-driven CO_2 reduction [366,367]. Mechanistic investigation reveals that the presence of single Co atoms in the MOF can greatly boost the electron-hole separation efficiency in porphyrin units [365]. Directional migration of photogenerated excitons from porphyrin to catalytic Co centers was revealed, thereby achieving supply of long-lived electrons for the reduction of CO_2 molecules adsorbed on Co centers [365].

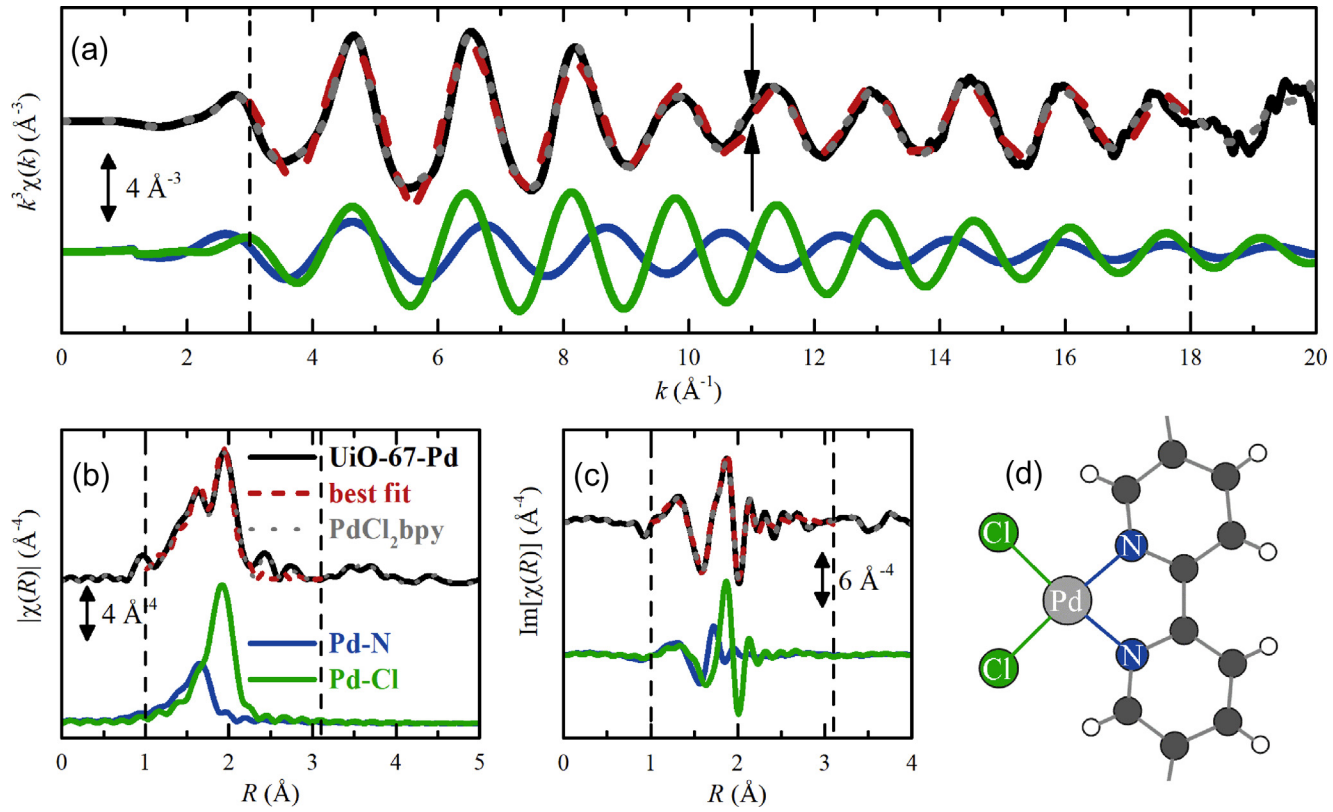

Fig. 7. k^2-Weighted $\chi(k)$ function (a), and the amplitudes (b) and imaginary parts (c) of their FT for experimental EXAFS data of UiO-67-Pd (solid black), $PdCl_2bpy$ linker (dotted grey) and the best fit (dashed red) by Pd-N (solid blue) and Pd-Cl (solid green) contributions, calculated using the model shown in panel (d). Reproduced from Ref. [346] by permission of The Royal Society of Chemistry.

MOF-525, formulated as $Zr_6O_4(OH)_4(TCPP\text{-}H_2)_3$ [TCPP = 4,4′,4″,4‴-(porphyrin-5,10,15,20-tetrayl) tetrabenzoate], which integrates Zr_6 clusters (the same as in UiO-66) and porphyrin-based molecular units into a 3D network, was selected as a MOF matrix for its excellent performance in CO_2 capture and visible-light utilization [365]. Coordinatively unsaturated Co sites were incorporated into the porphyrin units to generate a new composite, MOF-525-Co (See Fig. 8). Due to the highly porous structure of framework each active site is guaranteed simultaneous exposure to molecular CO_2 and can avoid aggregation of active sites due to the quite distant location of different active site inside the framework structure [365].

To probe the local coordination environment of the Co atom upon insertion within the framework, the Co K-edge XANES and EXAFS spectroscopies were implemented to the investigation of the system [365]. To answer the issue about formation of Co–Co bonding and revealed that most of the Co atoms exist as a mononuclear catalytic active centers Zhang et al. used WT EXAFS analysis of the Co K-edge [365]. The authors assign the signals from 1.0 to 5.0 Å to either Co-N(C) or Co–Co

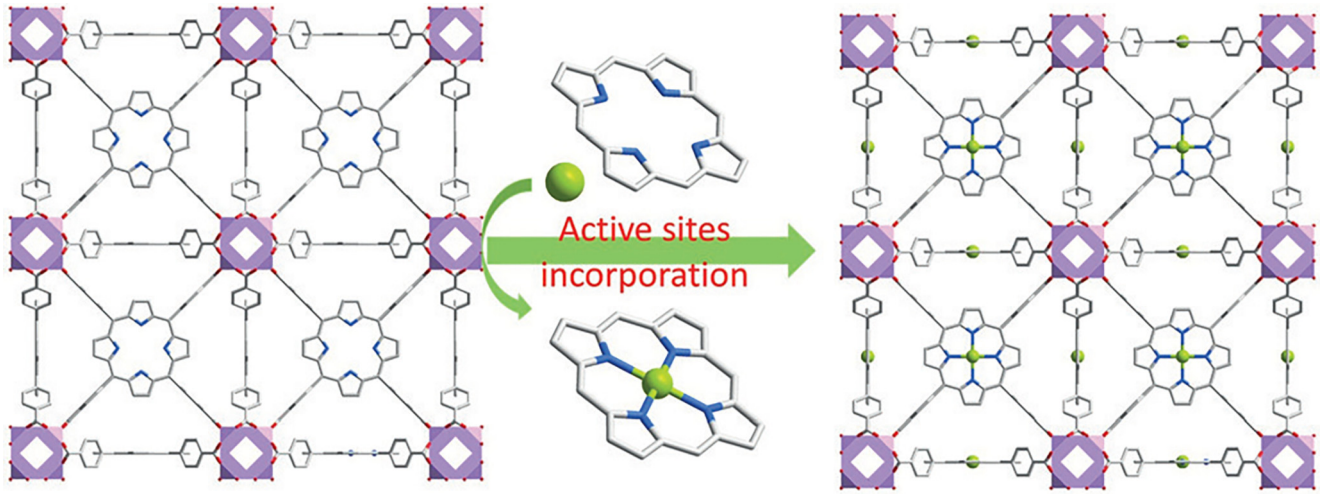

Fig. 8. 3D network of MOF-525-Co featuring a highly porous framework and incorporated active sites. Adopted from Ref. [365] by permission of John Wiley and Sons.

interactions is based on the detailed WT-EXAFS wavelet transform analysis.

For MOF-525-Co, a WT intensity maximum near 6.0 $Å^{-1}$ associated with a shoulder around 9.0 $Å^{-1}$ is well-resolved at 1.0–5.0 Å, this can be unambiguously assigned to the Co–N bond (see Fig. 9b). While the WT intensity maximum at 7.5 $Å^{-1}$ clearly observed for the Co foil (see Fig. 9a) and assigned with a Co–Co bonds is not detected in MOF-525-Co. EXAFS fitting support the conclusions of WT analysis and reveals that the coordination number of the nearest-neighbor N atoms surrounding the isolated Co atoms is 3.9 at 1.95 Å [365]. It could be also considered as an additional confirmation of square-planar configuration of Co in the newly developed MOF and the presence of unsaturated active sites for catalytic reaction [365]. In such way, WT-EXAFS analysis for MOF-525-Co reveals that Co atoms exist as a truly isolated atoms incorporated in the framework in the square-planar configuration.

Another case of implementation WT-EXAFS analysis on MOFs for photocatalysis reported by Yang An et al. [368]. So far, no MOFs has been reported to be a photocatalyst for overall water splitting. It is well known that compounds of Ni^{2+} ions are efficient cocatalysts for hydrogen production, and the amino groups of Al-ATA MOF present in the pores can act as ligand for the Ni^{2+} cations [369–371]. Yang An et al., employed Ni K-edge XANES and EXAFS spectroscopies for the investigation of Ni doped Al-ATA MOF which is considered to be promising photocatalyst for oxygen evolution from water, with the benzene ring of ATA^{2-} as the site for O_2 evolution [372].

The overall XANES profile of Al-ATA-Ni MOF is similar to that of $Ni(NO_3)_2$, with a much weaker pre-edge feature, which indicates that Ni atoms incorporated into framework are in oxidation state around +2 and octahedrally coordinated. Authors assign the signals from 1.0 to 4.0 Å to either Ni-N(O) or Ni–Al interaction based on the detailed WT-EXAFS analysis [368]. The WT intensity maximum around 4.5 $Å^{-1}$ is well resolved at a distance 1.6 Å has been assigned to the Ni–N and Ni–O bonding. There are no obvious signals detected that could be assigned to Ni–Ni bonding, which would have a WT maximum near 7.5 $Å^{-1}$ in *k* space and 2.14–2.58 Å in R space (See Fig. 10b). While the WT feature near 6.3 $Å^{-1}$ has been assigned to the Ni–Al bonding. It can be another example where WT analysis address the issue of formation single ion catalytically active sites, showing that Ni atoms incorporated into Al-ATA-Ni MOF are isolated atoms rather than forming Ni nanocrystals. The results of EXAFS fitting procedure confirms the octahedral coordination for Ni^{2+} ions the pores of Al-ATA-Ni MOF [368].

Shufang Ji et al., have applied WT-EXAFS analysis to clarified Ru_3 cluster formation in the ZIF-8 framework performing efficient oxidation of alcohols [373]. The active sites of the catalyst are represented by $Ru_3(CO)_{12}$ molecules within the cages of ZIF-8 framework. Uniform Ru_3/CN clusters stabilized by nitrogen species are formed during the further pyrolysis at 800 °C [373]. The Ru K-edge XANES show that the energy absorption threshold value of Ru_3/CN is higher than that of Ru foil and lower than of RuO_2, indicating that the Ru_3 clusters carry a positive charge. At the conventional EXAFS-FT curves there are two higher-shell peaks at distances of 2.3 and 3.0 Å that were observed for Ru_3/CN and were preliminary ascribed to Ru–Ru and Ru–C scattering, respectively. The further implementation of WT-EXAFS analysis allows to discriminate contribution from the heavy Ru and light C atoms (See Fig. 11a). WT contour plot of Ru_3/CN in the first shell shows one intensity maximum at ~4.2 $Å^{-1}$, associated with Ru–N scattering path. However for the higher coordination shell, WT counter plot shows two additional maxima at ~2.3 $Å^{-1}$ and 7.0 $Å^{-1}$, besides the intensity maxima at ~4.2 $Å^{-1}$, owing to Ru–C contributions. A complementary comparison of the q-space magnitudes for FEFF-calculated k^2-wieghted EXAFS paths was constructed (See Fig. 11b). The Ru–N(C) path shows the only one maximum near 4.2 $Å^{-1}$, while the Ru–Ru path shows one maxima near 8.7 $Å^{-1}$ associated with a shoulder around 3.8 $Å^{-1}$. However, with the Debye–Waller factors (σ^2) increased from 0.005 to 0.015 $Å^2$, an obvious shift of the Ru–Ru path maximum to 7.0 $Å^{-1}$ is clearly exhibited, suggesting that the WT maximum at 7.0 $Å^{-1}$ at the 2D plot can be ascribed to Ru–Ru scattering.

Thus, the Ru–N coordination and Ru–Ru metallic bonds of the Ru_3 triangular structures were detected, indicating that uniform Ru_3 clusters were atomically dispersed and stabilized by nitrogen species, as further confirmed by time-of-flight secondary ion mass spectrometry (TOF-SIMS) analysis [373].

However, the applications of WT-EXAFS analysis for porous materials are not limited by the dispersed single-site catalysts. One of the most specific issue which was addressed and partially solved by WT-EXAFS analysis is radionuclide sequestration in amorphous porous organic polymers (POPs) [374,375] and covalent organic frameworks (COFs) [376–378]. The investigation was performed by Qi Sun et al. [361], analyzing the U L_3-edge EXAFS signal obtained for POP-TpDb-AO and COF-TpDb-AO.

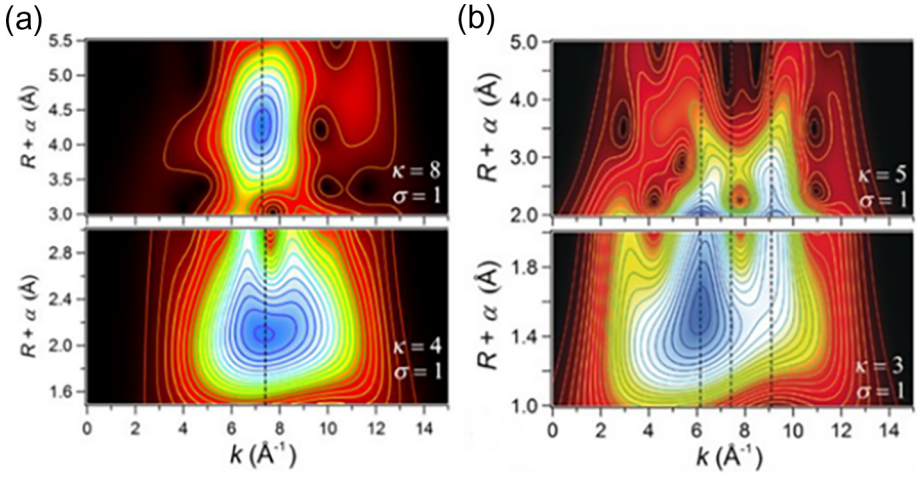

Fig. 9. (a) Wavelet transforms for the k^3-weighted Co K-edge EXAFS signals of Co foil and (b) of MOF-525-Co based on Morlet wavelets with optimum resolutions at the first (lower panel) and higher (upper panel) coordination shells. Vertical dashed lines denoting the *k*-space positions of the Co–N and Co–Co contributions. Adopted from Ref. [365] by permission of John Wiley and Sons.

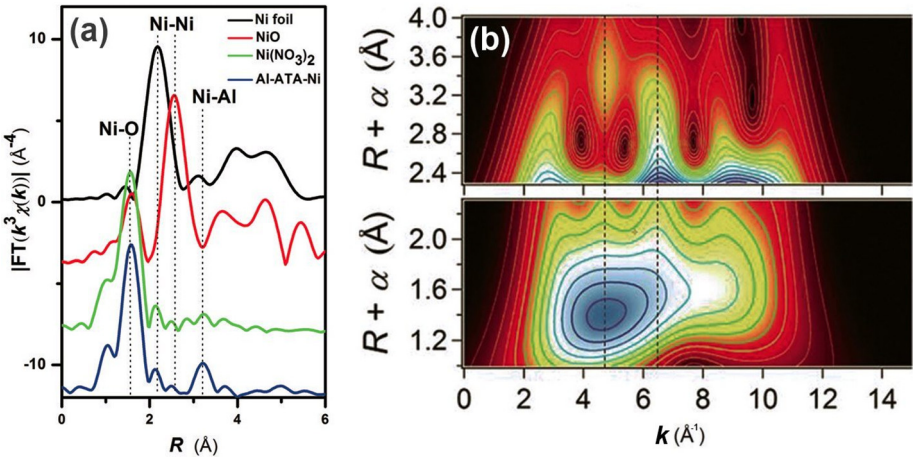

Fig. 10. (a) Conventional EXAFS Fourier transforms of Ni K-edge signal (b) Wavelet transforms for the k^3-weighted Ni K-edge EXAFS signals for the first (lower panel) and higher (upper panel) coordination shells of Al-ATA-Ni. Label on *x*-axis: k ($Å^{-1}$). Adopted from Ref. [368] by permission of John Wiley and Sons.

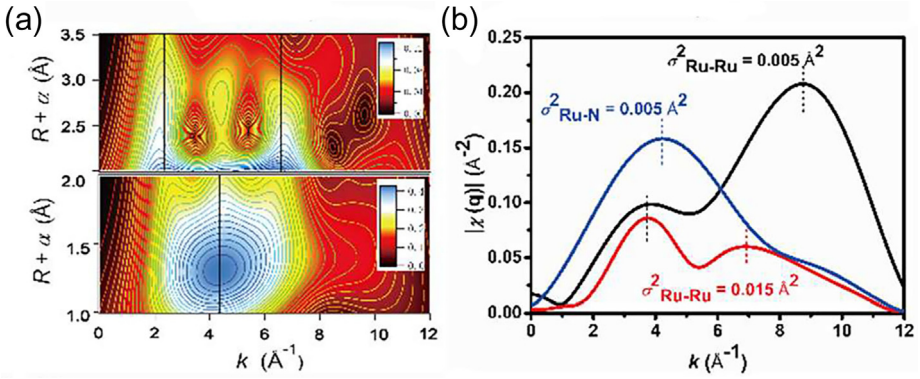

Fig. 11. (a) Wavelet transforms for the k^2-weighted Ru K-edge EXAFS signals for the high-coordination shells in Ru_3/CN. (b) Comparison of the q-space magnitudes for FEFF-calculated k^2-weighted EXAFS paths. Adopted with permission from Ref. [373]. Copyright 2017 American Chemical Society.

The wavelet transforms analysis demonstrate the extreme similarity between POP and COF systems (see Fig. 12), despite the increased information afforded through simultaneous inspection of both k- and R-signal components, suggests identical uranium-binding environment. Nevertheless, the observed improved performance of the COF-based adsorbents suggests that the well-oriented chelating groups on the COFs are more ready to bind with uranium species in comparison with the randomly populated form in the POPs [361].

3.3. MOFs as photocatalysts: time-resolved studies

MOFs are increasingly used in the field of photocatalysis addressing environmental and energy issues [128,379–387]. These

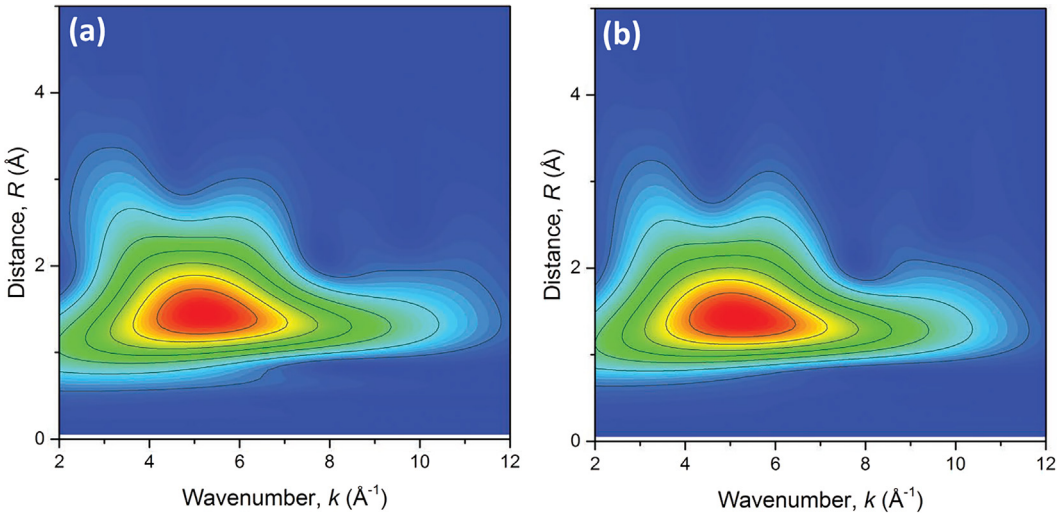

Fig. 12. U L_3-edge EXAFS k^2-weighted wavelet transforms analysis of (a) COF-TpDb-AO and (b) POP-TpDb-AO. Adopted from Ref. [361] by permission of John Wiley and Sons.

materials are believed capable to overcome the systematic restrictions immanent to traditional photocatalysts by exploiting their highly porous nanostructure and tunable semiconducting properties. There is a good number of review papers summarizing some recent achievements in employment of MOFs for solar energy conversion by photoredox catalysis [131,388], in the photo-driven removal of pollutants from wastewater [389], and as functional luminescent and photonic materials for sensing applications [390].

Han et al. [391] encapsulated polyoxometalate $[Co_4(H_2O)_2(PW_9O_{34})_2]^{10-}$ (CoPOM) in MIL-101(Cr) MOF for both photocatalytic and electrochemical catalytic water oxidation. To confirm that the structure of CoPOM after being encapsulated in MIL-101 is retained, authors measured the Co K-edge XANES of CoPOM/MIL-101 and CoPOM in comparison to several standards (Co_3O_4, $Co(OH)_2$ and $Co(NO_3)_2$). From the comparative analysis of curves, they attributed the observed shift of the absorption edge of CoPOM/MIL-101 to a higher energy by 0.9 eV to a guest–host interaction in the hybrid material. Different MOFs (like MIL-125, UiO-66, ZIF-8) functionalized with amine ($-NH_2$) group or semiconductor/metal nanoparticles were successfully tested to conduct the Cr(VI) reduction into Cr(III) [392].

There is a growing interest to combine Cu-BTC and TiO_2 in a pure form or as derivatives. In particular, a composite material combining HKUST-1 and SBA-15 grown solvothermally was proposed by Mosleh et al. [393] for photocatalytic degradation of toxic dyes under a blue LED light. Hollow Cu-TiO_2/C nanospheres from pyrolyzed core–shell SiO_2-HKUST-1-TiO_2 structures were found efficient in photocatalytic hydrogen production during the electrochemistry tests [394]. Although, authors of cited works link the questions of interfacial electron transfer with the structural peculiarities of the proposed systems, the information about local environment is still missing since the list of characterization methods rarely extends beyond XRD, TEM/SEM and optical spectroscopies (PL, UV–Vis and FTIR).

Xie et al. [395] reports on the ADA-Cd = $[Cd_2L_2(DMF)_2]\cdot 3H_2O$ where H_2L is (2E,2′E)-3,3′-(anthracene-9,10-diyl)diacrylic acid MOF as an effective sensitizer for anatase TiO_2 to achieve enhanced visible light photocatalytic performance. ADA-Cd acts as the antenna to harvest photons and inject generated electrons to CB of TiO_2.

Adjustable topological properties of MOFs offer unique opportunity for the photoswitchable applications of these materials. Optical control can be achieved either by light induced transformations in the metal centers (e.g. spin-crossover in MOF Fe(pyrazine)$Pt(CN)_4$ [396]) or by isomerization in the functional organic linkers (e.g. spiropyran-functionalized MOF-808 [397]). Practical applications of photoswitchable MOF include optically triggered release of molecular species from container [398,399]; selective gas adsorption [400]; tunable membrane separation [401] and photostimulated catalysis [402]. Large pores inside MOF can act as solid solvents for photoswitchable spiropyrans, as was observed for 1,3,3-Trimethylindolino-6′-nitrobenzopyrylospiran in MOF-5, MIL-68(In), and MIL-68(Ga) [403].

Appropriate methods should be used to follow time evolution of the atomic and electronic structure of the material after short and intense laser pump pulse. Optical pump–probe experiments are often used to characterize photodynamic properties of MOFs. In the work [404] authors unravel the photodynamic of Nile Red (NR) interacting with Al–ITQ-HB nanostructure. Time-resolved experiments provided emission lifetimes of the interacting monomers, H- and J-type aggregates. This study showed that the structural transformations of Nile Red molecule in Al–ITQ-HB MOF upon light irradiation depend on its location within the material. Infrared spectroscopy is also sensitive to the atomic structure and local coordination of molecules inside MOF. Time-resolved transient infrared spectroscopy in the picosecond time domain following 400 nm irradiation of $M(CO)_3$(diimine)X (M = Re, Mn) MOF was used to characterize metal to ligand charge transfer and photoejection of carbon monoxide [405]. Subsecond infrared and Raman spectroscopy were used to follow the mer-isomer product formation during the photolysis of ReMn in a KBr disk (ReMn = $[Mn(DMF)_2[LRe(CO)_3Cl]]_\infty$, L = 2,2′-bipyridine-5,5′-dicarboxylate, DMF = N,N dimethylformamide).

There are few examples of time-resolved structural analysis of MOF under irradiation. A four-dimension electron microscopy diffraction was applied for spin crossover transitions in single crystal of MOF Fe(pyrazine)$Pt(CN)_4$ [396]. X-ray studies using scattering methods up to date cover only sub-second time domain [19,406,407] and focus mainly on the formation process of the MOF crystals during synthesis. Modern X-ray absorption and RIXS techniques developed nowadays at X-ray free electron lasers [408,409] are still challenging for the *in situ* applications to delicate and degradable MOF structures. However numerous optical pump X-ray probe studies of the metallorganic molecules [210,410–412], which are building blocks of MOFs, foresee a development of appropriate environmental conditions for MOF at existing synchrotron and XFEL beamlines.

3.4. MOFs as materials for gas sorption and storage

Due to structural properties of MOFs one the most obvious applications of them are sorption [34,38,413–416] and separation [31,417]. Nowadays highly efficient sorption and removal of pollutants and toxic ions is serious task from the environmental point of view.

In order to investigate physical and chemical transformations and structural dynamics of three commercial MOFs (Cu-BTC, Fe-BTC and ZIF-8) during the CO_2 adsorption experiments, XAFS measurements were performed on different reaction steps (as-synthesized sample, activated, after CO_2 adsorption/desorption) [418]. The activation and CO_2 gas adsorption process in the rht-type MOF were investigated on the molecular level using several spectroscopic characterization methods [419].

Although elemental halogens play key roles in a range of industrial process, most of reports on gas sorption and storage in MOFs are mentioned oxidizing or corrosive gases (O_2, NO, SO_2, NH_3). Tulchinsky et al. [203] represent the first example of reversible halogen uptake and release with a MOF. Using a combination of XANES, EXAFS techniques and theoretical calculations were shown that Br_2 and Cl_2 reversible oxidize Co(II) centers in Co_2Cl_2BTDD (1) (BTDD = bis(1H-1,2,3-triazolo[4,5-b],[4,5-i])dibenzo[1,4]dioxin) to form terminal cobalt(III) halides in $Co_2Cl_2X_2$BTDD (X = Cl, Br).

MOFs could be used as solid-phase sorbents to remove heavy metals by the introduction of suitable functionals groups, for example many effective sorbents for Hg(II) based on MOFs or COFs (covalent organic frameworks) have been developed based on strong Hg-S interactions. The possibility of reversible uptake of Cd (II) by MOF FJI-H9 was shown in [420].

Considering the mobility, radioactivity, and high toxicity of uranium, together with its indispensable role in nuclear energy, uranium sequestration was thus chosen as a proof-of-concept study to demonstrate the potential applications of COFs in waste management and nuclear source enrichment to safeguard energy development. To gain more insight into the coordination environment of uranium in both COF-TpDb-AO and POP-TpDb-AO Bai et al. [361] employed XAFS spectroscopy collected at the U L_3-absorption edge (17.166 keV). Inspection of the data suggests the U(VI) coordination environment is similar between the two porous frameworks, and reasonable fits are obtained from applying the same uranyl-benzamidoxime η^2 binding motif model to both COF-TpDb-AO and POP-TpDb- AO. Two distinct U–O distances are required within the equatorial coordination plane, consistent

with η^2 binding; however, the spectral resolution of the data (≈0.2 Å) precludes definitive assignment of the uranium coordination environment. Nevertheless, the successful simultaneous fitting of the EXAFS data sets with the same structure model, in conjunction with affording refined parameters within experimental uncertainty of each other, demonstrates a common uranium-binding mode.

Zhang et al. [421,422] used XAFS techniques to investigate the local coordination around the U(VI) in MIL-101(Cr) with different ethylenediamine (ED) functionalities before and after U(VI) sorption. As shown in Fig. 13, similar XANES patterns consisting of a strong main peak (I) and a shoulder II can be seen in all U(VI)-loaded MIL-101(Cr) samples, disclosing the bipyramid skeletal structure of uranyl. The increase of the ED ratio led to changes in the areas of peaks II/III. The energy positions of the peaks II and III depend on the U–Oax and U–Oeq bond distances. Peaks in Fig. 3b correspond to the single scattering paths of oxygen (axial) and the ligand (equatorial). The numbers of axial and equatorial coordinated atoms were two and six, respectively. The authors found that U(VI) was mainly coordinated to the amine groups in ED-MIL-101(Cr), while physical adsorption was dominant in pristine MIL-101(Cr). The key advantage of XAFS is that it is element specific and always detectable. The application of XAFS tools will be largely carried out for understanding the speciation and microstructures of toxic/radioactive metal ions adsorbed onto the surfaces of MOF-based materials with the increasing demand for molecular-scale metal ion-speciation information and the increasing sophistication of the XAFS tools.

EXAFS data were recorded in order to determine the coordination environment of U(VI)-loaded MIL-101-NH_2, MIL-101-ED and MIL-101-DETA [422]. It is observed that, on the one hand, spectra MIL-101-ED and MIL-101-DETA have almost the same oscillation mode and the same intense FT peaks in the range of 1–6, whereas spectrum for MIL-101-NH_2 shows a clear difference in intensity of the FT peak at ~2 Å. This indicated that U(VI) sorption on MIL-101-ED and MIL-101-DETA occurs in the same way but is slightly different from that on MIL-101-NH_2. On the other hand, all these spectra are distinct from for the reference of U(VI) hydroxide precipitate, revealing the absence of such an incidental species under the experimental conditions.

The $[Cu_3(BTC)_2(H_2O)_3]_n$ (where BTC is benzene-1,3,5-tricarboxylate) or simply HKUST-1 was introduced to scientific community in 1999 by Chui et al. [423]. Describing the attractive features of obtained face-centered cubic crystals with a 3D system of pores, authors stressed out the control of dimensionality as a key factor to successful synthesis of MOF. Under a room-temperature synthesis conditions the copper trimesate system usually turned into the polymeric ensembles of low dimensionality due to ligation of aqua groups to square-pyramidal Cu^{2+} ion. Only synthesis at a higher temperature (180 °C in the reported case) ensured a loss of terminal ancillary ligands (with just one aqua molecule left per a metal center) and establishing of a 3D polymeric network. The same report provided a brief description of dimeric cupric tetracarboxylate units based on a single-crystal analysis; the Cu–Cu internuclear separation was 2.628(2) Å and the Cu–OH_2 bonds were 2.165(8) Å.

The water molecules in the first coordination sphere of Cu ions, if removed, form coordinative vacancy on Cu(II) species, allowing usage of the material for the capture and storage of guest molecules, such as hydrogen [424–426]. Substantial potential of such application stimulated the XAS studies of the copper species in HKUST-1. Both XANES and EXFAS were collected for the MOF and three standards (metallic Cu, Cu_2O, and CuO) in fluorescence or transmission mode in the regions of the Cu K edge (8979 eV) at room temperature on a synchrotron source. Although, the edge positions were confirming the Cu(II) oxidation state, the offset of 0.4 eV for the as-synthesized HKUST-1 (solvothermal process at 110 °C for 18 h) revealed that Cu ions were not entirely surrounded by four oxygens from BTC linkers and formed covalent bonds with hydroxyls. The EXAFS studies were focused on analysis of Cu–O distances in HKUST-1 between the metal atom and the oxygen of the axial aqua ligands. The Cu–O length of 1.94 Å for the fresh MOF was found slightly changing to 1.96 upon heating at 200 °C.

The reaction of the framework to the dehydration process occurring under outgassing at 180 °C was investigated with a set of different techniques (including a synchrotron-quality XAS) by Prestipino et al. [424]. Considering the evolution of the XANES features when passing from hydrated to dehydrated state of HKUST-1, a change in the coordination of Cu(II) was justified by a decrease of the white line, by promotion of the 1s → 4p dipolar shakedown

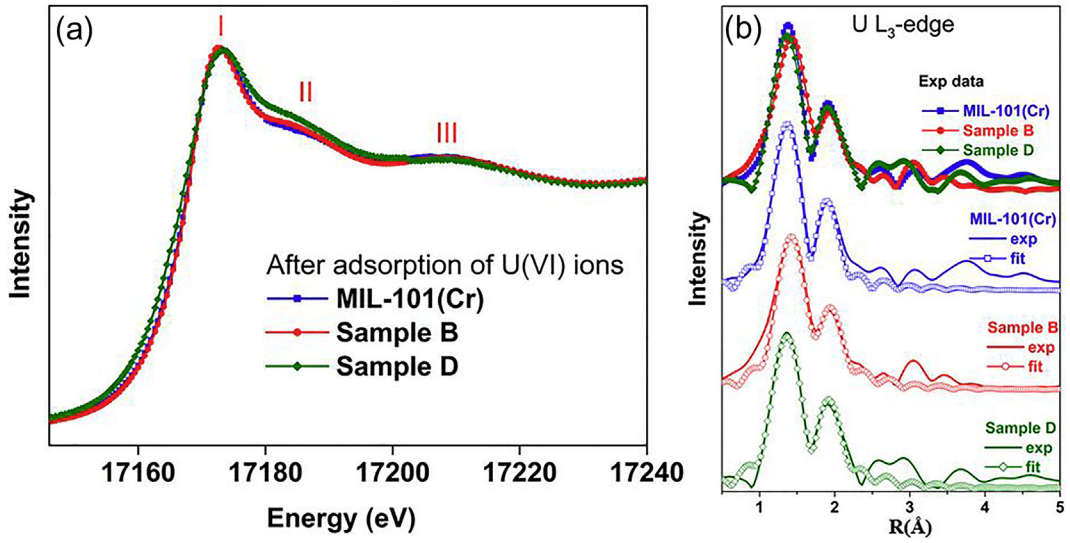

Fig. 13. (a) Comparison of experimental U L3-edge XANES spectra for pristine MIL-101(Cr), and different ED contents grafting ED-MIL-101(Cr) samples after the adsorption of U(VI). (b) Experimental Fourier Transform at of the U L3-edge EXAFS data for different samples and their corresponding fits. (c) J. Y. Zhang et al. reprinted from Ref. [421]. Used under Creative Commons Attribution 4.0 International License (http://creativecommons.org/licenses/by/4.0).

transition, and by perturbation of the 1s → 3d quadrupolar transition. The observed changes in both intensity and position of characteristic bands, because of the removal of axial water molecules, led to a higher covalency of ligand-copper bond over its ionicity. For the theoretical fitting of the experimental EXAFS signals (*k*-weighted Fourier back-transformed) the scattering environment of so-called paddle-wheel units formed by four carboxylate groups coordinating two Cu(II) ions was described as the hydrated $[Cu_2C_4O_8](H_2O)_2$ or the dehydrated $[Cu_2C_4O_8]$ cage (cornerstone). The analysis demonstrated that dehydration results in shortening of all the scattering paths in the $[Cu_2C_4O_8]$ cage. The bond lengths were calculated (with accuracy of ±0.02 Å) as 2.19 Å for the Cu–OH_2 bond in the hydrated state (as-synthesized HKUST-1) and 2.64 Å for the Cu–Cu separation, the last reducing to 2.50 Å upon removal of coordinated water molecules.

Removal of water molecules axially bonded to the Cu(II) dimers forms the Lewis acid copper sites accessible for chemisorption of molecules having basic character. A careful study of NH_3 adsorption on coordinatively unsaturated copper sites was performed with several characterization techniques by Borfecchia et al. [201]. Similar to other reports, the XANES spectra (Fig. 14) are typical of Cu(II) species, exhibiting the edge jump at 8990 eV and two pre-edge peaks at ca. 8976 eV and ca. 8986 eV due to the 1s → 3d and 1s → 4p transitions, respectively. For the starting hydrated HKUST-1, the best agreement between the experimental (measured at the Cu K edge at the ESRF) and simulated (using FEFF8.4 code on the optimized XRPD structure) curve was reached with some shortening of the Cu–OH_2 bond and slight general contraction of all other distances. Upon water removal, the changes in XANES profile resembles those observed in previous studies of dehydration. After the interaction of the activated MOF with NH_3, a new pre-edge peak appears at ca. 8983 eV accompanied by slight changes in the whole spectral profile. The simulation (by substituting the water molecules with two NH_3 molecules) demonstrated that the intensity of pre-edge peak at ca. 8986 eV is proportional to the Cu–NH_3 distance (2.3 Å) and splitting of the white line is caused by distortion of carbonyl groups. These structural changes are similar to what has been observed in the case of water but quantitatively bigger.

The unsaturated Cu(II) ions in the dehydrated HKUST-1 may serve as charge-dense binding sites even for nonpolar molecules. Investigating the CO_2 adsorption/desorption of Cu-BTC, Fe-BTC and ZIF-8, Du et al. [418] concluded that the CO_2 capture is mainly governed by the physical driving force. Surprisingly, the dehydrated Cu-BTC showed 5–7 times higher absorption amount of CO_2 compared to other two MOFs (all possess similar BET surface areas). Based on the differences on the fitted coordination number and distance for Cu–O shell between activation and sorption steps (processed from a synchrotron XAS data), the adsorption of CO_2 molecule to Cu^{2+} center by forming a chemical Cu–O bond was assumed.

Following a Modular Chemistry concept [30], many carboxylate MOFs, isoreticular to HKUST-1, have been designed so far by selecting a secondary building unit with another metal [427] or substituting a linker [428]. There is a growing number of hybrid MOFs under study with partial substitution.

Mixed-linker MOFs based on the Cu-BTC structure were synthesized by Marx et al. [429] with full or partial replacement of BTC by pyridine-3,5-dicarboxylate (PyDC) XAS measurements on the Cu-BTC samples observed the known trends in modification of spectral profiles upon the loss of a coordinated water molecule resulting in a strengthening and shortening of the Cu–O carboxylate bonds. For the Cu-BTC-PyDC samples, the intensities of the white line in XANES and the amplitude in the Fourier-transformed EXAFS spectra were found decreasing with increasing amount of PyDC (up to 50%). These tendencies evidenced a decrease in the coordination number of the copper atoms and an increase in the electron density at them. The Cu–Cu separation (2.61 Å) becomes smaller by 0.3 Å, while amount of axially bonded water does not change for up to 30% PyDC. The presence of nitrate or hydroxide ions in the unit was supposed to compensate a positive charge due to missed carboxylate group, although, it was not possible to prove with EXAFs.

3.5. MOFs for energy storage

Ability to store guest molecules and ions in the pores make MOFs useful for energy applications, in particular for the hydrogen storage, cathode materials for Li-ion and sodium batteries, supercapacitors. Dennis Sheberla et al. [430], studied the conductive MOF electrodes for stable electrochemical double layer supercapacitors (EDLC) with high areal capacitance. Due to their

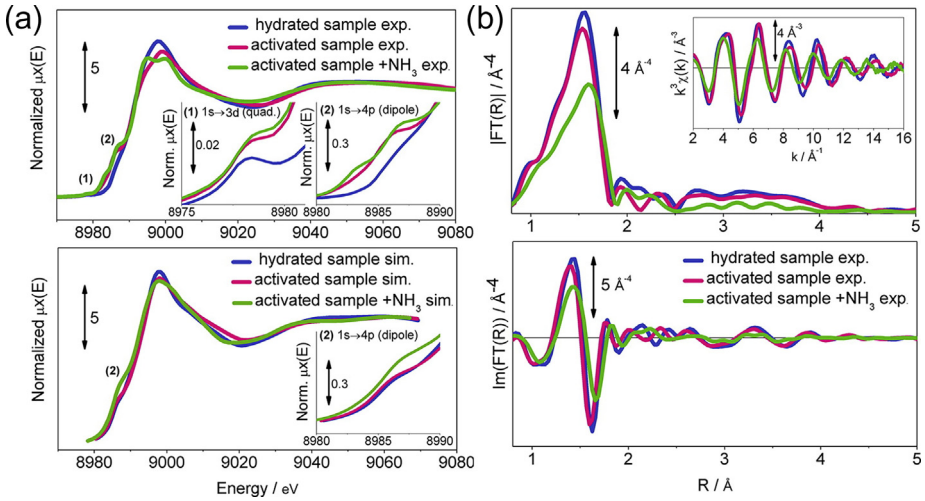

Fig. 14. (a) Experimental (top panel) and simulated (bottom panel) XANES spectra of HKUST-1 as-prepared (blue line), activated (pink line), and activated + NH_3 (green line). The insets report magnifications of the 1s → 3d quadrupolar transition (1) and of the shakedown 1s → 4p transition (2). (b) Qualitative comparison between experimental EXAFS data for as-prepared and activated HKUST-1, and for the activated sample upon contact with 50 mbar of ammonia. Modulus (top panel) and imaginary part (bottom panel) of the FT of the k^3-weighted χ(k) functions reported in the inset for the as-prepared (blue line), activated (pink line), and activated + NH_3 (green line) sample. The inset in the top part reports the corresponding k^3 χ(k) functions. Reprinted with permission from Ref. [201] Copyright (2012) American Chemical Society.

high-power density and cyclic stability, EDLCs together with lithium ion batteries will favor development of the green energy sources, electric transport and smart power grids. The MOFs have high porosity, which is attractive for the storage of electrochemically active species, however practical application is still limited due to poor electrical conductivity. So far this prevented the use of these materials as active electrodes in EDLCs. However, it was found that recently synthesized Ni_3(2,3,6,7,10,11-hexaiminotriphenylene)$_2$ (Ni_3(HITP)$_2$) MOF [430] shown in Fig. 15, has appropriate value of electrical conductivity to be used solely as electrode material in an EDLC without conductive additives of other binders.

Authors revealed a working potential window of ~1.0 V for Ni_3(HITP)$_2$ and after 0.5 V a quasi-reversible oxidation process was observed. The microscopic origin of the oxidation processes was studied by means of X-ray absorption spectroscopy at the Ni K-edge. Corresponding spectra are shown in Fig. 16 and Fig. 17. Material subjected to anodic polarization at 1 V (Fig. 16) revealed no changes in the Ni K-edge position and shape of near edge fine structure, thus local coordination around Ni remained unchanged. This observation suggests that the quasi-reversible oxidation at ~0.7 V is related rather to HITP linker than to Ni.

Degradation processes in the local atomic structure around Ni was observed upon cycling above 1.5 V. Clear changes were observed both for negative and positive electrodes as follows from Fig. 17.

JaeWook Shin, et al, [431] studied the electrochemical performance of a MIL 101(Fe) MOF as a material for a lithium ion battery electrode. Upon cycling iron changed its oxidation state between Fe^{2+} and Fe^{3+} however this process was not reversible over many cycles. Authors use *ex situ* and operando X-ray absorption spectroscopy above Fe K-edge. *Ex situ* measurements were performed since a different behavior was observed for the material subjected to the intense synchrotron radiation due to irreversible oxidation of Fe^{2+} into Fe^{3+}. Fig. 18b shows chemical shift of the Fe K-edge to lower energy during lithiation and then reversibly shift back upon de-lithiation. Such chemical shift during lithiation is consistent with the reduction of Fe^{3+} to a superposition of phases with divalent and trivalent ions of Fe^{3+} and Fe^{2+}. Upon de-lithiation, the mixed valence state is oxidized back to Fe^{3+}.

The Fourier transform of the EXAFS region in Fig. 18c shows the radial distribution of nearest neighbor atoms around iron. Intensity of the maximum around 1.5 Å correlates with the number of

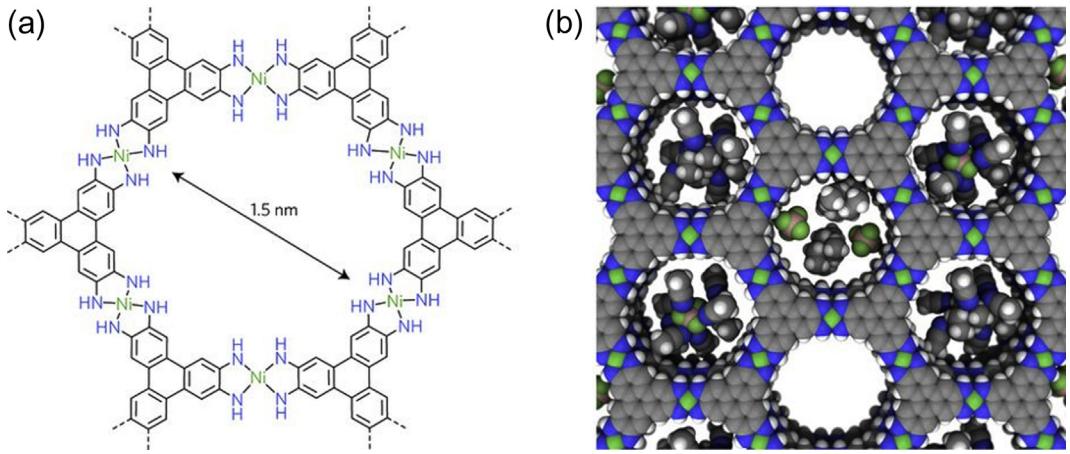

Fig. 15. Schematic representation if Ni_3(HITP)$_2$ MOF a, Molecular structure of Ni_3(HITP)$_2$ with 1.5 nm pore size Panel b compares size of pores, electrolyte Et_4N^+ and BF_4^- ions, and acetonitrile solvent molecules Green, lime, blue, grey, brown, and white spheres represent Ni, F, N, C, B, and H atoms, respectively. Reprinted from Ref. [430] with permission from Nature Publishing Group, copyright 2016.

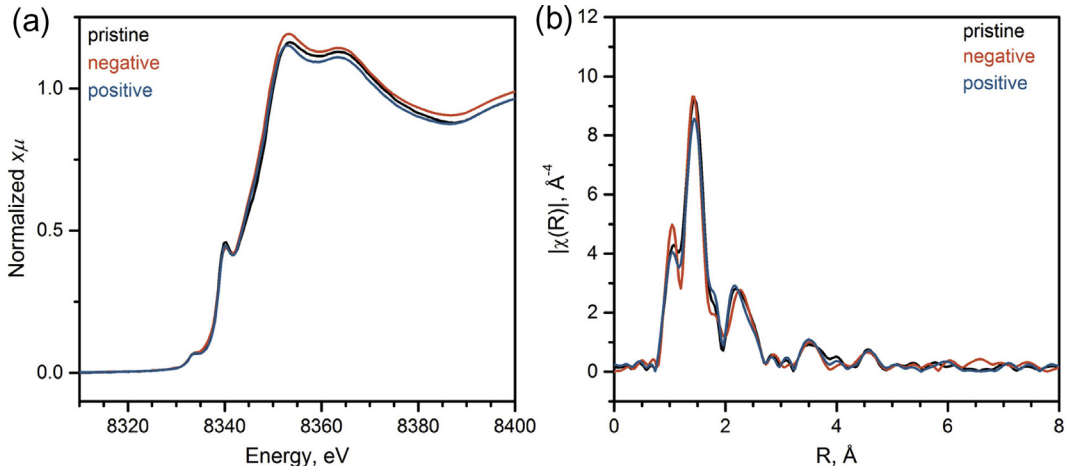

Fig. 16. (a) Ni K-edge near edge fine structure and (b) k^3-weighted Fourier transform of the EXAFS measured for of Ni_3(HITP)$_2$ material at electrodes. Negative label corresponds to the charge up to −0.6 V vs Ag/AgCl while positive is 1.0 V vs Ag/AgCl. Reprinted from Ref. [430] with permission from Nature Publishing Group, copyright 2016.

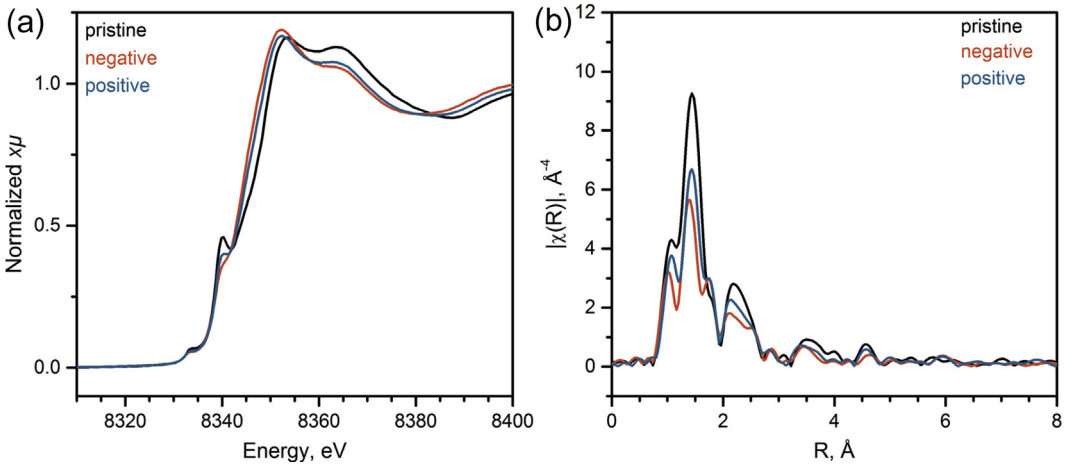

Fig. 17. Degradation of $Ni_3(HITP)_2$ electrodes upon deep cycling up to 1.7 V. Panel (c) shows Ni K-edge XANES and (d) k^3-weighted Fourier transform of the EXAFS. Working conditions for cycling were 2 A g^{-1} between 0.0 and 1.7 V over 5000 cycles. Reprinted from Ref. [430] with permission from Nature Publishing Group, copyright 2016.

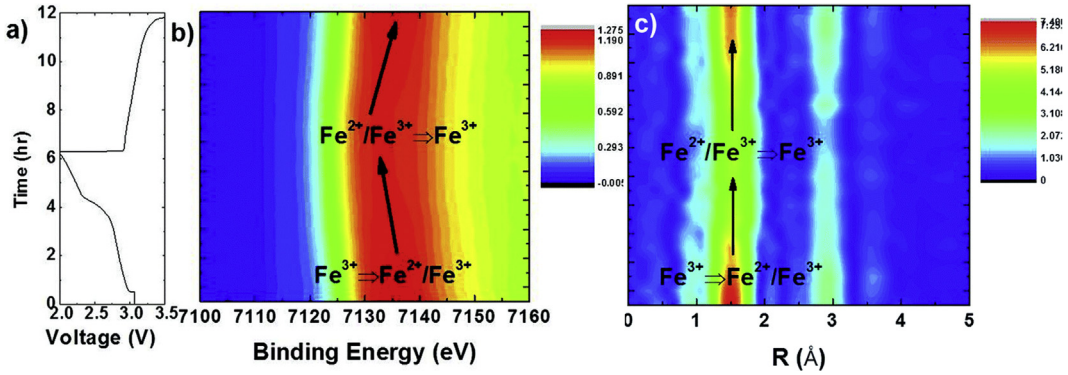

Fig. 18. *Operando* XANES of MIL-101(Fe). (a) Voltage profile with respect to the in operando XAS scanning time. (b) The contour plot of the in operando XAS region versus time indicates a reversible change in the absorption edge position and thus Fe oxidation state. (c) Contour plot of the Fourier transformed EXAFS region of the in operando XAS data. Reprinted from Ref. [431] with permission from the Royal Society of Chemistry, copyright 2015.

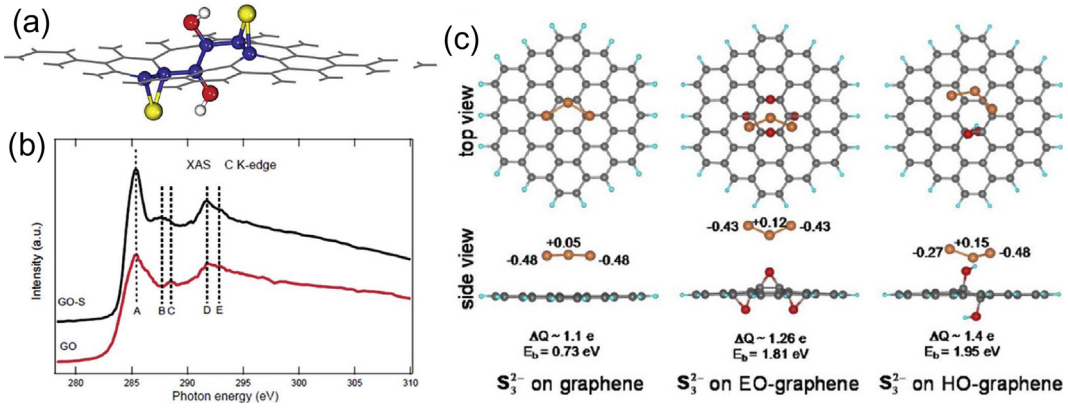

Fig. 19. C K-edge XANES for the graphene oxide material before and after interaction with polysulfides and corresponding structural models obtained from DFT simulations (electron exchange and binding energy values shown). Reproduced with permission from Ref. [432]. Copyright 2015, The Electrochemistry Society.

neighbors in the first coordination shell. The intensity of the corresponding peak decreases upon Li insertion and then increases again upon Li extraction. Such behavior can be attributed to a reversible replacement of chlorine atom by one oxygen atom from an electrolyte solvent molecule upon full lithiation.

Pores of MOFs can be used to encapsulate polysulfides for the cyclic stability of lithium sulfur batteries. X-ray absorption spectroscopy can be a useful tool to study chemical bonds between sulfur and organic linkers of MOF. There are no applications of soft x-rays to such composite materials however existing studies cover

interaction of sulfur with carbon atoms in graphene sheets. Quan Pang, et al, [432] using C K-edge X-ray absorption spectroscopy revealed a strong chemical interaction between sulfur host materials and lithium polysulfides along with formation of C–S bond (Fig. 19).

Chao Li. et al. [433] fabricated Mn- and Ni-based ultrathin MOF nanosheets ('Mn-UMOFNs' and 'Ni-UMOFNs') using ultrasonic approach. Synthesized materials were studied upon Li cycling with O K-edge XANES using total electron yield (TEY) mode. The obtained Mn-UMOFNs exhibit capacity up to 1187 mAh g^{-1} at 100 mA g^{-1} charge/discharge current for 100 cycles. Fig. 20 shows *ex situ* XAS for different potential at galvanostatic electrochemical profile. The most sensitive to the Li insertion were the pre-edge region between 530 and 537 eV which corresponds to the excitations of O 1 s electrons to the hybridized state of O-2p and Mn-3d orbitals and two peaks at 539.82 and 543.03 eV which originate from hybridized O-2p and Mn-4sp orbitals.

Another wide application of MOF is the synthesis of amorphous carbon shell with embedded metallic nanoparticles which result from the decomposition of the MOF. XianHe Meng, et al. [434] synthesized porous Ni@C derived from bimetallic MOFs and used this material to improve $LiBH_4$ dehydrogenation properties. First, the Ni K-edge XAS was used to prove that Ni^{2+} ions substitute Zn^{2+} ions in the bimetallic MOF-5 (see Fig. 21a). Secondly formation of metal

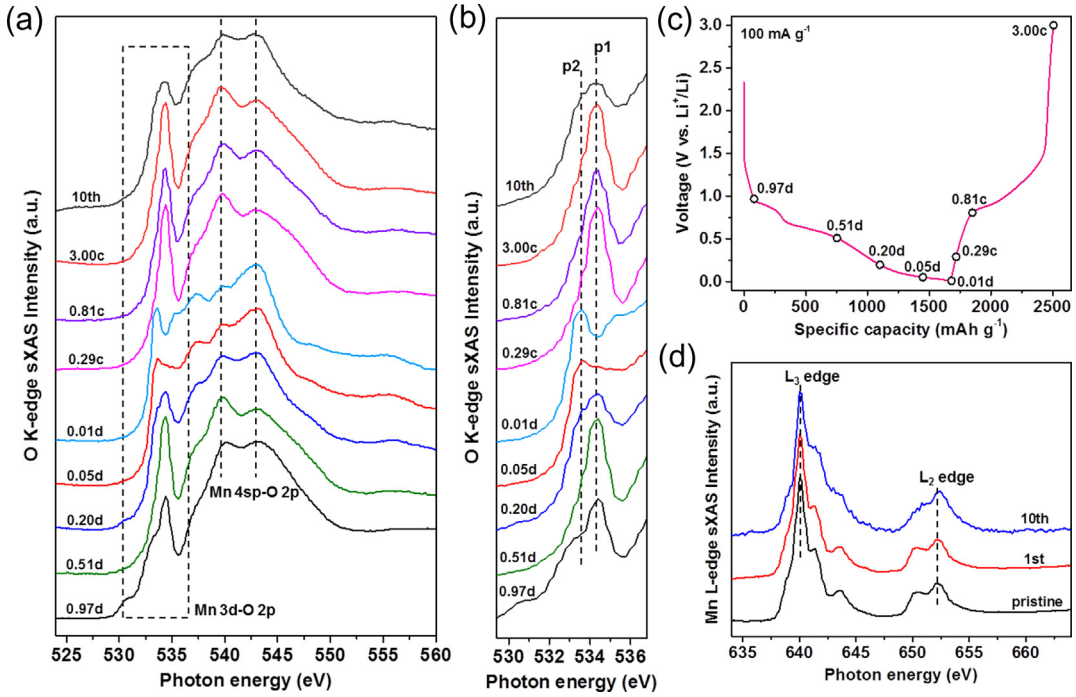

Fig. 20. (a) *Ex situ* O K-edge X-ray absorption spectra measured in total electron yield mode for the Mn-UMOFNs at the points marked in panel (c). (b) Enlarged pre-edge region for the spectra in panel (a). Panel (d) shows Mn L-edge spectra of the sample before and galvanostatic charge/discharge cycles. Reprinted from Ref. [433] with permission from the American Chemical Society, copyright 2017.

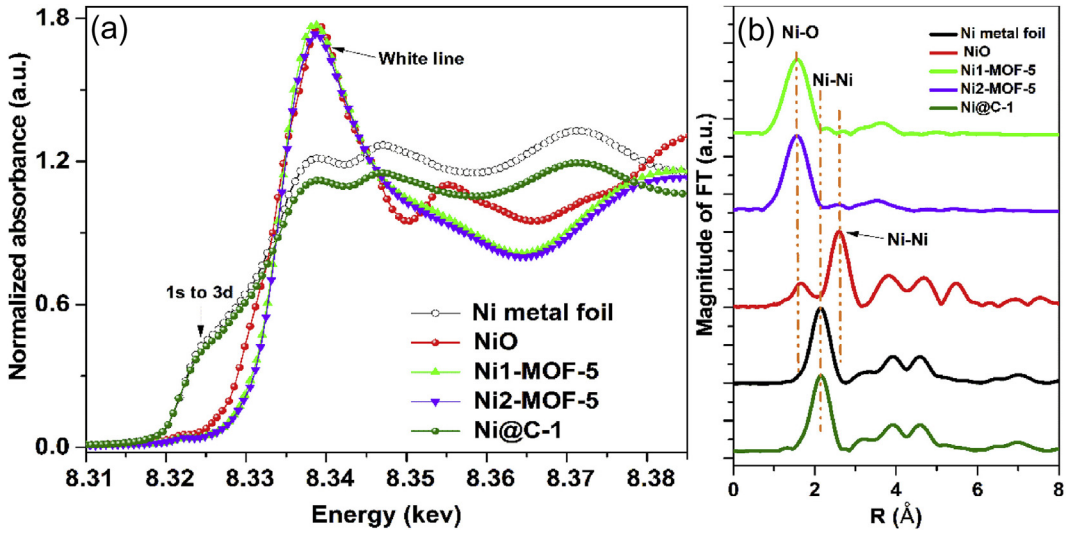

Fig. 21. (a) X-ray absorption spectra above Ni K-edge for Ni metal foil, NiO, Ni1-MOF-5, Ni2-MOF-5, and Ni@C-1 and (b) corresponding phase corrected Fourier transformed-EXAFS spectra. Reprinted from Ref. [434] with permission from the Elsevier, copyright 2018.

nanoparticles was evidenced from the comparison of the spectrum from Ni@C composite with the spectrum of metallic foil and corresponding radial distribution functions (Fig. 21b). In the Fourier transformed data the first oxygen coordination shell in Ni1-MOF-5 and Ni2-MOF-5 is located at 1.6 Å whereas the Ni-O distance equals 1.7 Å for NiO. Detailed analysis of the EXAFS data can provide additional information about Ni-Ni and Ni-Zn pairs in $[Zn_4O]^{6+}$ clusters after Ni/Zn substitution. The FT-EXAFS of Ni@C-1(after 1000 °C treatment in Ar of MOF structures) shows fine structure in spectra similar to those in the spectrum for Ni metal foil with Ni-Ni distance equal to 2.0 Å.

4. Conclusions and perspectives

High brilliance of modern synchrotron radiation sources makes it possible to shift a paradigm of X-ray nanocharacterization in materials science from the *ex situ* studies of materials to the studies of the processes involving materials transformations (*in situ* studies) [158–160,164,435-437]. The necessity of bridging the gap between the real industrial applications and laboratory studies push even more sophisticated modification of the process studies developing operando experimental set-ups [255,258-260,262, 264,438–457], eventually able to couple XAFS with additional spectroscopic or scattering technique [263,458–463]. In such cases the process under the study follows real technological conditions and, thus, the researchers could reach the important information on the fine details of local atomic and electronic structures of advanced materials in real technological applications [464].

High energy-resolved fluorescence detected (HERFD) XAS increases the spectral resolution well below the core–hole width limit and gives additional site selectivity, but at the serious expense of the count rate [465–479]. The experimental set-up used for HERFD XANES data collection also allows high resolution X-ray emission spectroscopy (XES) spectra to be performed. XES, like X-ray photoelectron spectroscopy (XPS) and ultraviolet photoelectron spectroscopy (UPS), probes the occupied density of states (DOS) and it this complementary to XANES, that probes the unoccupied DOS with the advantage that vacuum conditions needed by XPS and UPS are not required and that XES can probe the whole volume of the investigated material [262,449,471,474,480–498]. Moreover, valence-to core XES probing the molecular orbital that contributes to the chemical bond, it is able to distinguish neighbors atoms of similar Z, like (C, O and N [262,474]), (Al and P [491]) etc... succeeding where other techniques like EXAFS, XANES and XRD fails.

The modern vector in the XAFS techniques development is the need for significant enhancement of time, spatial and spectroscopic resolution. With the X-ray free electron lasers (XFEL) it is possible to reach the time-resolution well below 100 fs [499,500], but the X-ray spectral bandwidth of these machines is less than 1%. XANES measurements with XFEL have been successfully demonstrated [501], however for EXAFS they seem like an unreachable goal so far. Synchrotron radiation diffraction limited storage rings are expected to provide unique possibilities for focusing and imaging [212], including XAS mapping [502].

All these cutting-edge characterization techniques are available for understanding the structural and electronic properties of MOFs materials as well as for understanding their working mechanisms when they are used for any of the applications discussed in this review.

Acknowledgements

This work was supported through Megagrant 14.Y26.31.0001 from the Government of the Russian Federation for State Support of Scientific Research conducted under the guidance of leading scientists. M. A. Soldatov is grateful for the scholarship of the President of the Russian Federation for young scientists № СП-377.2016.4.

References

[1] A.K. Cheetham, G. Ferey, T. Loiseau, Angew. Chem. Int., Edit. 38 (1999) 3268.
[2] M. Eddaoudi, D.B. Moler, H.L. Li, B.L. Chen, T.M. Reineke, M. O'Keeffe, O.M. Yaghi, Acc. Chem. Res. 34 (2001) 319.
[3] G. Ferey, Chem. Mater. 13 (2001) 3084.
[4] S.L. James, Chem. Soc. Rev. 32 (2003) 276.
[5] D. Bradshaw, J.B. Claridge, E.J. Cussen, T.J. Prior, M.J. Rosseinsky, Acc. Chem. Res. 38 (2005) 273.
[6] G. Ferey, Chem. Soc. Rev. 37 (2008) 191.
[7] M. O'Keeffe, Chem. Soc. Rev. 38 (2009) 1215.
[8] R. Prajapati, L. Mishra, K. Kimura, P. Raghavaiah, Polyhedron 28 (2009) 600.
[9] H. Furukawa, N. Ko, Y.B. Go, N. Aratani, S.B. Choi, E. Choi, A.O. Yazaydin, R.Q. Snurr, M. O'Keeffe, J. Kim, O.M. Yaghi, Science 329 (2010) 424.
[10] O.K. Farha, J.T. Hupp, Acc. Chem. Res. 43 (2010) 1166.
[11] O. Shekhah, J. Liu, R.A. Fischer, C. Woll, Chem. Soc. Rev. 40 (2011) 1081.
[12] N. Stock, S. Biswas, Chem. Rev. 112 (2012) 933.
[13] W.M. Xuan, C.F. Zhu, Y. Liu, Y. Cui, Chem. Soc. Rev. 41 (2012) 1677.
[14] Q.L. Zhu, Q. Xu, Chem. Soc. Rev. 43 (2014) 5468.
[15] F.X. Coudert, A.H. Fuchs, Coord. Chem. Rev. 307 (2016) 211.
[16] V.V. Butova, M.A. Soldatov, A.A. Guda, K.A. Lomachenko, C. Lamberti, Russ. Chem. Rev. 85 (2016) 280.
[17] J.X. Liu, C. Woll, Chem. Soc. Rev. 46 (2017) 5730.
[18] M. Rubio-Martinez, C. Avci-Camur, A.W. Thornton, I. Imaz, D. Maspoch, M.R. Hill, Chem. Soc. Rev. 46 (2017) 3453.
[19] M.J. Van Vleet, T.T. Weng, X.Y. Li, J.R. Schmidt, Chem. Rev. 118 (2018) 3681.
[20] C.A. Stackhouse, S.Q. Ma, Polyhedron 145 (2018) 154.
[21] B. Valizadeh, T.N. Nguyen, K.C. Stylianou, Polyhedron 145 (2018) 1.
[22] U. Müller, M. Schubert, F. Teich, H. Puetter, K. Schierle-Arndt, J. Pastre, J. Mater. Chem. 16 (2006) 626.
[23] A.U. Czaja, N. Trukhan, U. Muller, Chem. Soc. Rev. 38 (2009) 1284.
[24] M. Shah, M.C. McCarthy, S. Sachdeva, A.K. Lee, H.K. Jeong, Ind. Eng. Chem. Res. 51 (2012) 2179.
[25] S.L. Qiu, M. Xue, G.S. Zhu, Chem. Soc. Rev. 43 (2014) 6116.
[26] K.A. Cychosz, R. Ahmad, A.J. Matzger, Chem. Sci. 1 (2010) 293.
[27] A. Ahmed, N. Hodgson, M. Barrow, R. Clowes, C.M. Robertson, A. Steiner, P. McKeown, D. Bradshaw, P. Myers, H.F. Zhang, J. Mater. Chem. A 2 (2014) 9085.
[28] L.L. Wen, X.Y. Xu, K.L. Lv, Y.M. Huang, X.F. Zheng, L. Zhou, R.Q. Sun, D.F. Li, A.C. S. Appl, Mater. Interfaces 7 (2015) 4449.
[29] M. Kondo, T. Yoshitomi, K. Seki, H. Matsuzaka, S. Kitagawa, Angew. Chem., Int. Edit. Engl. 36 (1997) 1725.
[30] M. Eddaoudi, J. Kim, N. Rosi, D. Vodak, J. Wachter, M. Keeffe, O.M. Yaghi, Science 295 (2002) 469.
[31] M. Dinca, J.R. Long, J. Am. Chem. Soc. 127 (2005) 9376.
[32] M. Dinca, A.F. Yu, J.R. Long, J. Am. Chem. Soc. 128 (2006) 8904.
[33] P.D.C. Dietzel, R.E. Johnsen, H. Fjellvag, S. Bordiga, E. Groppo, S. Chavan, R. Blom, Chem. Commun. (2008) 5125.
[34] J.G. Vitillo, L. Regli, S. Chavan, G. Ricchiardi, G. Spoto, P.D.C. Dietzel, S. Bordiga, A. Zecchina, J. Am. Chem. Soc. 130 (2008) 8386.
[35] O.K. Farha, A.O. Yazaydin, I. Eryazici, C.D. Malliakas, B.G. Hauser, M.G. Kanatzidis, S.T. Nguyen, R.Q. Snurr, J.T. Hupp, Nat. Chem. 2 (2010) 944.
[36] S.Q. Ma, H.C. Zhou, Chem. Commun. 46 (2010) 44.
[37] K. Sumida, S. Horike, S.S. Kaye, Z.R. Herm, W.L. Queen, C.M. Brown, F. Grandjean, G.J. Long, A. Dailly, J.R. Long, Chem. Sci. 1 (2010) 184.
[38] K. Sumida, D.L. Rogow, J.A. Mason, T.M. McDonald, E.D. Bloch, Z.R. Herm, T.H. Bae, J.R. Long, Chem. Rev. 112 (2012) 724.
[39] J.A. Mason, M. Veenstra, J.R. Long, Chem. Sci. 5 (2014) 32.
[40] D. Alezi, Y. Belmabkhout, M. Suyetin, P.M. Bhatt, L.J. Weselinski, V. Solovyeva, K. Adil, I. Spanopoulos, P.N. Trikalitis, A.H. Emwas, M. Eddaoudi, J. Am. Chem. Soc 137 (2015) 13308.
[41] B. Seoane, J. Coronas, I. Gascon, M.E. Benavides, O. Karvan, J. Caro, F. Kapteijn, J. Gascon, Chem. Soc. Rev. 44 (2015) 2421.
[42] M.S. Shah, M. Tsapatsis, J.I. Siepmann, Chem. Rev. 117 (2017) 9755.
[43] X.C. Yang, Q. Xu, Cryst. Growth Des. 17 (2017) 1450.
[44] H. Li, K.C. Wang, Y.J. Sun, C.T. Lollar, J.L. Li, H.C. Zhou, Mater. Today 21 (2018) 108.
[45] S. Jakobsen, D. Gianolio, D.S. Wragg, M.H. Nilsen, H. Emerich, S. Bordiga, C. Lamberti, U. Olsbye, M. Tilset, K.P. Lillerud, Phys. Rev. B 86 (2012) 125429.
[46] E. Barea, C. Montoro, J.A.R. Navarro, Chem. Soc. Rev. 43 (2014) 5419.
[47] J.B. DeCoste, G.W. Peterson, Chem. Rev. 114 (2014) 5695.
[48] N.S. Bobbitt, M.L. Mendonca, A.J. Howarth, T. Islamoglu, J.T. Hupp, O.K. Farha, R.Q. Snurr, Chem. Soc. Rev. 46 (2017) 3357.
[49] B.Y. Li, X.L. Dong, H. Wang, D.X. Ma, K. Tan, Z. Shi, Y.J. Chabal, Y. Han, J. Li, Faraday Discuss 201 (2017) 47.
[50] S. Waitschat, D. Frohlich, H. Reinsch, H. Terraschke, K.A. Lomachenko, C. Lamberti, H. Kummer, T. Helling, M. Baumgartner, S. Henningerb, N. Stock, Dalton Trans. 47 (2018) 1062.
[51] J. Li, X.X. Wang, G.X. Zhao, C.L. Chen, Z.F. Chai, A. Alsaedi, T. Hayat, X.K. Wang, Chem. Soc. Rev. 47 (2018) 2322.

[52] P. Horcajada, C. Serre, M. Vallet-Regi, M. Sebban, F. Taulelle, G. Ferey, Angew. Chem., Int. Edit. 45 (2006) 5974.
[53] B. Xiao, P.S. Wheatley, X.B. Zhao, A.J. Fletcher, S. Fox, A.G. Rossi, I.L. Megson, S. Bordiga, L. Regli, K.M. Thomas, R.E. Morris, J. Am. Chem. Soc. 129 (2007) 1203.
[54] P. Horcajada, T. Chalati, C. Serre, B. Gillet, C. Sebrie, T. Baati, J.F. Eubank, D. Heurtaux, P. Clayette, C. Kreuz, J.S. Chang, Y.K. Hwang, V. Marsaud, P.N. Bories, L. Cynober, S. Gil, G. Ferey, P. Couvreur, R. Gref, Nat. Mater. 9 (2010) 172.
[55] J. Della Rocca, D.M. Liu, W.B. Lin, Acc. Chem. Res. 44 (2011) 957.
[56] W. Cai, C.C. Chu, G. Liu, Y.X.J. Wang, Small 11 (2015) 4806.
[57] M. Ibrahim, R. Sabouni, G.A. Husseini, Curr. Med. Chem. 24 (2017) 193.
[58] M.H. Teplerisky, M. Fantham, P. Li, T.C. Wang, J.P. Mehta, L.J. Young, P.Z. Moghadam, J.T. Hupp, O.K. Farha, C.F. Kaminski, D. Fairen-Jimenez, J. Am. Chem. Soc. 139 (2017) 7522.
[59] J.Q. Sha, X.Y. Yang, L.J. Sun, X.M. Zhang, S.X. Li, J.S. Li, N. Sheng, Polyhedron 127 (2017) 396.
[60] X.M. Jia, Z.Y. Yang, Y.J. Wang, Y. Chen, H.T. Yuan, H.Y. Chen, X.X. Xu, X.Q. Gao, Z.Z. Liang, Y. Sun, J.R. Li, H.Q. Zheng, R. Cao, ChemMedChem 13 (2018) 400.
[61] I.A. Lazaro, S.A. Lazaro, R.S. Forgan, Chem. Commun. 54 (2018) 2792.
[62] L. Wang, M. Zheng, Z.G. Xie, J. Mat. Chem. B 6 (2018) 707.
[63] L.E. Kreno, K. Leong, O.K. Farha, M. Allendorf, R.P. Van Duyne, J.T. Hupp, Chem. Rev. 112 (2012) 1105.
[64] I. Stassen, B. Bueken, H. Reinsch, J.F.M. Oudenhoven, D. Wouters, J. Hajek, V. Van Speybroeck, N. Stock, P.M. Vereecken, R. Van Schaijk, D. De Vos, R. Ameloot, Chem. Sci. 7 (2016) 5827.
[65] I. Stassen, N. Burtch, A. Talin, P. Falcaro, M. Allendorf, R. Ameloot, Chem. Soc. Rev. 46 (2017) 3185.
[66] C. Serre, F. Millange, C. Thouvenot, N. Gardant, F. Pelle, G. Ferey, J. Mater. Chem. 14 (2004) 1540.
[67] S. Bordiga, C. Lamberti, G. Ricchiardi, L. Regli, F. Bonino, A. Damin, K.P. Lillerud, M. Bjorgen, A. Zecchina, Chem. Commun. (2004) 2300.
[68] M.D. Allendorf, C.A. Bauer, R.K. Bhakta, R.J.T. Houk, Chem. Soc. Rev. 38 (2009) 1330.
[69] K.L. Zhang, W. Liang, Y. Chang, L.M. Yuan, S.W. Ng, Polyhedron 28 (2009) 647.
[70] T.P. Hu, L.J. Liu, X.L. Lv, X.H. Chen, H.Y. He, F.N. Dai, G.Q. Zhang, D.F. Sun, Polyhedron 29 (2010) 296.
[71] G. Lu, J.T. Hupp, J. Am. Chem. Soc. 132 (2010) 7832.
[72] W.Q. Kan, J. Yang, Y.Y. Liu, J.F. Ma, Polyhedron 30 (2011) 2106.
[73] R.Q. Fan, L.Y. Wang, H. Chen, G.P. Zhou, Y.L. Yang, W. Hasi, W.W. Cao, Polyhedron 33 (2012) 90.
[74] X.Z. Song, S.Y. Song, S.N. Zhao, Z.M. Hao, M. Zhu, X. Meng, L.L. Wu, H.J. Zhang, Adv. Funct. Mater. 24 (2014) 4034.
[75] B. Yan, Acc. Chem. Res. 50 (2017) 2789.
[76] R. Medishetty, J.K. Zareba, D. Mayer, M. Samoc, R.A. Fischer, Chem. Soc. Rev. 46 (2017) 4976.
[77] X.F. Wang, Y. Pan, Z. Li, X. Li, S.L. Qiu, M. Xue, Polyhedron 122 (2017) 55.
[78] A. Chidambaram, K.C. Stylianou, Inorg. Chem. Front. 5 (2018) 979.
[79] L.T. Liu, Y.L. Zhou, S. Liu, M.T. Xu, ChemElectroChem 5 (2018) 6.
[80] Y.M. Zhang, S. Yuan, G. Day, X. Wang, X.Y. Yang, H.C. Zhou, Coord. Chem. Rev. 354 (2018) 28.
[81] D. Maspoch, D. Ruiz-Molina, K. Wurst, N. Domingo, M. Cavallini, F. Biscarini, J. Tejada, C. Rovira, J. Veciana, Nat. Mater. 2 (2003) 190.
[82] D. Maspoch, D. Ruiz-Molina, J. Veciana, J. Mater. Chem. 14 (2004) 2713.
[83] K.M.L. Taylor, W.J. Rieter, W.B. Lin, J. Am. Chem. Soc. 130 (2008) 14358.
[84] M. Kurmoo, Chem. Soc. Rev. 38 (2009) 1353.
[85] S.S. Pedro, P. Brandao, F.N. Shi, J.C.G. Tedesco, M.S. Reis, Polyhedron 81 (2014) 210.
[86] N.L. Torad, M. Hu, S. Ishihara, H. Sukegawa, A.A. Belik, M. Imura, K. Ariga, Y. Sakka, Y. Yamauchi, Small 10 (2014) 2096.
[87] M. Raizada, F. Sama, M. Ashafaq, M. Shahid, M. Khalid, M. Ahmad, Z.A. Siddiqi, Polyhedron 139 (2018) 131.
[88] Y.P. Wang, X.G. Li, S.L. Liu, J.N. Fry, H.P. Cheng, Phys. Rev. B 97 (2018) 115419.
[89] G. Ferey, F. Millange, M. Morcrette, C. Serre, M.L. Doublet, J.M. Greneche, J.M. Tarascon, Angew. Chem., Int. Edit. 46 (2007) 3259.
[90] S. Horike, D. Umeyama, S. Kitagawa, Acc. Chem. Res. 46 (2013) 2376.
[91] J.M. Taylor, K.W. Dawson, G.K.H. Shimizu, J. Am. Chem. Soc 135 (2013) 1193.
[92] M. Sadakiyo, H. Kasai, K. Kato, M. Takata, M. Yamauchi, J. Am. Chem. Soc. 136 (2014) 1702.
[93] X.C. Xie, K.J. Huang, X. Wu, J. Mater. Chem. A 6 (2018) 6754.
[94] H. Zhang, X.M. Liu, Y. Wu, C. Guan, A.K. Cheetham, J. Wang, Chem. Commun. 54 (2018) 5268.
[95] M. Alvaro, E. Carbonell, B. Ferrer, F. Xamena, H. Garcia, Chem. Eur. J. 13 (2007) 5106.
[96] F. Xamena, A. Corma, H. Garcia, J. Phys. Chem. C 111 (2007) 80.
[97] C.G. Silva, A. Corma, H. Garcia, J. Mater. Chem. 20 (2010) 3141.
[98] M. Usman, S. Mendiratta, K.L. Lu, Adv. Mater. 29 (2017) 5.
[99] L.P. Tang, L.M. Tang, H. Geng, Y.P. Yi, Z.M. Wei, K.Q. Chen, H.X. Deng, Appl. Phys. Lett. 112 (2018) 5.
[100] M.D. Allendorf, A. Schwartzberg, V. Stavila, A.A. Talin, Chem. Eur. J. 17 (2011) 11372.
[101] V. Stavila, A.A. Talin, M.D. Allendorf, Chem. Soc. Rev. 43 (2014) 5994.
[102] X.G. Yang, X.Q. Lin, Y.S. Zhao, D.P. Yan, Chem. Eur. J. 24 (2018) 6484.
[103] J. Yang, P.X. Xiong, C. Zheng, H.Y. Qiu, M.D. Wei, J. Mater. Chem. A 2 (2014) 16640.
[104] L. Wang, X. Feng, L.T. Ren, Q.H. Piao, J.Q. Zhong, Y.B. Wang, H.W. Li, Y.F. Chen, B. Wang, J. Am. Chem. Soc. 137 (2015) 4920.
[105] R.R. Salunkhe, Y.V. Kaneti, J. Kim, J.H. Kim, Y. Yamauchi, Acc. Chem. Res. 49 (2016) 2796.
[106] R.R. Salunkhe, Y.V. Kaneti, Y. Yamauchi, ACS Nano 11 (2017) 5293.
[107] S. Eslava, L.P. Zhang, S. Esconjauregui, J.W. Yang, K. Vanstreels, M.R. Baklanov, E. Saiz, Chem. Mater. 25 (2013) 27.
[108] S. Mendiratta, M. Usman, K.L. Lu, Coord. Chem. Rev. 360 (2018) 77.
[109] J. Lee, O.K. Farha, J. Roberts, K.A. Scheidt, S.T. Nguyen, J.T. Hupp, Chem. Soc. Rev. 38 (2009) 1450.
[110] D. Farrusseng, S. Aguado, C. Pinel, Angew. Chem., Int. Edit. 48 (2009) 7502.
[111] L.Q. Ma, C. Abney, W.B. Lin, Chem. Soc. Rev. 38 (2009) 1248.
[112] A. Corma, H. Garcıa, F.X. Llabres i Xamena, Chem. Rev. 110 (2010) 4606.
[113] M. Yoon, R. Srirambalaji, K. Kim, Chem. Rev. 112 (2012) 1196.
[114] F.X. Llabrés i Xamena, J. Gascón, Metal organic frameworks as heterogeneous catalysts, R. Soc. Chem. Cambridge (2013).
[115] D.J. Xiao, E.D. Bloch, J.A. Mason, W.L. Queen, M.R. Hudson, N. Planas, J. Borycz, A.L. Dzubak, P. Verma, K. Lee, F. Bonino, V. Crocella, J. Yano, S. Bordiga, D.G. Truhlar, L. Gagliardi, C.M. Brown, J.R. Long, Nat. Chem. 6 (2014) 590.
[116] J.W. Liu, L.F. Chen, H. Cui, J.Y. Zhang, L. Zhang, C.Y. Su, Chem. Soc. Rev. 43 (2014) 6011.
[117] G.W. Zhan, H.C. Zeng, Coord. Chem. Rev. 320 (2016) 181.
[118] Y.B. Huang, J. Liang, X.S. Wang, R. Cao, Chem. Soc. Rev. 46 (2017) 126.
[119] S.N. Zhao, X.Z. Song, S.Y. Song, H.J. Zhang, Coord. Chem. Rev. 337 (2017) 80.
[120] Y.Z. Chen, R. Zhang, L. Jiao, H.L. Jiang, Coord. Chem. Rev. 362 (2018) 1.
[121] T.W. Murinzi, E. Hosten, G.M. Watkins, Polyhedron 137 (2017) 188.
[122] A.D.S. Barbosa, D. Juliao, D.M. Fernandes, A.F. Peixoto, C. Freire, B. de Castro, C. M. Granadeiro, S.S. Balula, L. Cunha-Silva, Polyhedron 127 (2017) 464.
[123] S. Halder, P. Ghosh, C. Rizzoli, P. Banerjee, P. Roy, Polyhedron 123 (2017) 217.
[124] E.S. Gutterod, S. Oien-Odegaard, K. Bossers, A.E. Nieuwelink, M. Manzoli, L. Braglia, A. Lazzarini, E. Borfecchia, S. Ahmadigoltapeh, B. Bouchevreau, B.T. Lonstad-Bleken, R. Henry, C. Lamberti, S. Bordiga, B.M. Weckhuysen, K.P. Lillerud, U. Olsbye, Ind. Eng. Chem. Res. 56 (2017) 13207.
[125] S. Smolders, K.A. Lomachenko, B. Bueken, A. Struyf, A.L. Bugaev, C. Atzori, N. Stock, C. Lamberti, M.B.J. Roeffaers, D.E. De Vos, ChemPhysChem 19 (2018) 373.
[126] S. Kempahanumakkagari, K. Vellingiri, A. Deep, E.E. Kwon, N. Bolan, K.H. Kim, Coord. Chem. Rev. 357 (2018) 105.
[127] C. Wang, Z.G. Xie, K.E. deKrafft, W.L. Lin, J. Am. Chem. Soc 133 (2011) 13445.
[128] Y.H. Fu, D.R. Sun, Y.J. Chen, R.K. Huang, Z.X. Ding, X.Z. Fu, Z.H. Li, Angew. Chem., Int. Edit. 51 (2012) 3364.
[129] A. Fateeva, P.A. Chater, C.P. Ireland, A.A. Tahir, Y.Z. Khimyak, P.V. Wiper, J.R. Darwent, M.J. Rosseinsky, Angew. Chem., Int. Edit. 51 (2012) 7440.
[130] J.L. Wang, C. Wang, W.B. Lin, ACS Catal. 2 (2012) 2630.
[131] T. Zhang, W. Lin, Chem. Soc. Rev. 43 (2014) 5982.
[132] D.Y. Shi, C. He, B. Qi, C. Chen, J.Y. Niu, C.Y. Duan, Chem. Sci. 6 (2015) 1035.
[133] H. Wang, X.Z. Yuan, Y. Wu, G.M. Zeng, X.H. Chen, L.J. Leng, H. Li, Appl. Catal. B Environ. 174 (2015) 445.
[134] S.B. Wang, X.C. Wang, Small 11 (2015) 3097.
[135] A. Dhakshinamoorthy, A.M. Asiri, H. Garcia, Angew. Chem., Int. Edit. 55 (2016) 5414.
[136] B.L. Yan, L.J. Zhang, Z.Y. Tang, M. Al-Mamun, H.J. Zhao, X.T. Su, Appl. Catal. B-Environ. 218 (2017) 743.
[137] J.W. Liu, Y.Z. Fan, X. Li, Z.W. Wei, Y.W. Xu, L. Zhang, C.Y. Su, Appl. Catal. B Environ. 231 (2018) 173.
[138] Y. Chen, V. Lykourinou, T. Hoang, L.J. Ming, S.Q. Ma, Inorg. Chem. 51 (2012) 9156.
[139] Y.H. Shih, S.H. Lo, N.S. Yang, B. Singco, Y.J. Cheng, C.Y. Wu, I.H. Chang, H.Y. Huang, C.H. Lin, ChemPlusChem 77 (2012) 982.
[140] J. Huo, J. Aguilera-Sigalat, S. El-Hankari, D. Bradshaw, Chem. Sci. 6 (2015) 1938.
[141] F.K. Shieh, S.C. Wang, C.I. Yen, C.C. Wu, S. Dutta, L.Y. Chou, J.V. Morabito, P. Hu, M.H. Hsu, K.C.W. Wu, C.K. Tsung, J. Am. Chem. Soc. 137 (2015) 4276.
[142] H.M. He, H.B. Han, H. Shi, Y.Y. Tian, F.X. Sun, Y. Song, Q.S. Li, G.S. Zhu, A.C.S. Appl, Mater. Interfaces 8 (2016) 24517.
[143] X.Z. Lian, Y. Fang, E. Joseph, Q. Wang, J.L. Li, S. Banerjee, C. Lollar, X. Wang, H.C. Zhou, Chem. Soc. Rev. 46 (2017) 3386.
[144] A. Samui, S.K. Sahu, New J. Chem. 42 (2018) 4192.
[145] G. Ferey, C. Serre, Chem. Soc. Rev. 38 (2009) 1280.
[146] J.R. Long, O.M. Yaghi, Chem. Soc. Rev. 38 (2009) 1213.
[147] S. Oien-Odegaard, G.C. Shearer, D.S. Wragg, K.P. Lillerud, Chem. Soc. Rev. 46 (2017) 4867.
[148] K.C. Szeto, K.P. Lillerud, M. Tilset, M. Bjorgen, C. Prestipino, A. Zecchina, C. Lamberti, S. Bordiga, J. Phys. Chem. B 110 (2006) 21509.
[149] K.C. Szeto, C. Prestipino, C. Lamberti, A. Zecchina, S. Bordiga, M. Bjorgen, M. Tilset, K.P. Lillerud, Chem. Mater. 19 (2007) 211.
[150] J. Hafizovic, M. Bjorgen, U. Olsbye, P.D.C. Dietzel, S. Bordiga, C. Prestipino, C. Lamberti, K.P. Lillerud, J. Am. Chem. Soc. 129 (2007) 3612.
[151] N. Masciocchi, S. Galli, V. Colombo, A. Maspero, G. Palmisano, B. Seyyedi, C. Lamberti, S. Bordiga, J. Am. Chem. Soc. 132 (2010) 7902.
[152] J.H. Cavka, S. Jakobsen, U. Olsbye, N. Guillou, C. Lamberti, S. Bordiga, K.P. Lillerud, J. Am. Chem. Soc. 130 (2008) 13850.
[153] L. Valenzano, B. Civalleri, S. Bordiga, M.H. Nilsen, S. Jakobsen, K.-P. Lillerud, C. Lamberti, Chem. Mater. 23 (2011) 1700.
[154] S. Chavan, J.G. Vitillo, D. Gianolio, O. Zavorotynska, B. Civalleri, S. Jakobsen, M. H. Nilsen, L. Valenzano, C. Lamberti, K.P. Lillerud, S. Bordiga, Phys. Chem. Chem. Phys. 14 (2012) 1614.

[155] D.C. Koningsberger, R. Prins, X-ray absorption: principles, applications, techniques of EXAFS, SEXAFS, and XANES, John Wiley and Sons, New York, 1988.
[156] A. Filipponi, A. Di Cicco, C.R. Natoli, Phys. Rev. B 52 (1995) 15122.
[157] J.J. Rehr, R.C. Albers, Rev. Mod. Phys. 72 (2000) 621.
[158] S. Bordiga, E. Groppo, G. Agostini, J.A. van Bokhoven, C. Lamberti, Chem. Rev. 113 (2013) 1736.
[159] C. Garino, E. Borfecchia, R. Gobetto, J.A. van Bokhoven, C. Lamberti, Coord. Chem. Rev. 277 (2014) 130.
[160] J.A. van Bokhoven, C. Lamberti, X-Ray Absorption and X-Ray Emission Spectroscopy: Theory and Applications, Wiley, Chichester, 2016.
[161] L. Mino, G. Agostini, E. Borfecchia, D. Gianolio, A. Piovano, E. Gallo, C. Lamberti, J. Phys. D Appl. Phys. 46 (2013) 72.
[162] J.J. Kas, K. Jorissen, J.J. Rehr, Real-Space Multiple-Scattering Theory of X-Ray Spectra, in: J.A. van Bokhoven, C. Lamberti (Eds.), X-Ray Absorption and X-Ray Emission Spectroscopy: Theory and Applications, John Wiley & Sons, Chichester (UK), 2016, p. 51.
[163] C. Lamberti, J.A. van Bokhoven, Introduction: Historical Perspective on XAS, Wiley, 2016.
[164] S. Bordiga, F. Bonino, K.P. Lillerud, C. Lamberti, Chem. Soc. Rev. 39 (2010) 4885.
[165] E. Borfecchia, D. Gianolio, G. Agostini, S. Bordiga, C. Lamberti, Characterization of MOFs. 2. Long and local range order structural determination of MOFs by combining EXAFS and diffraction techniques, in: F. Xamena, J. Gascon (Eds.), Metal Organic Frameworks as Heterogeneous Catalysts, Royal Soc Chemistry, Cambridge, 2013, p. 143.
[166] E. Borfecchia, L. Braglia, F. Bonino, S. Bordiga, S. Øien, U. Olsbye, K.P. Lillerud, J. A. van Bokhoven, K.A. Lomachenko, A.A. Guda, M.A. Soldatov, C. Lamberti, Probing structure and reactivity of metal centers in metal-organic frameworks by XAS techniques, in: Y. Iwasawa, K. Asakura, M. Tada (Eds.), XAFS Techniques for Catalysts, Nanomaterials, and Surfaces, Springer, Berlin, 2017, p. 397.
[167] F. Bonino, S. Chavan, J.G. Vitillo, E. Groppo, G. Agostini, C. Lamberti, P.D.C. Dietzel, C. Prestipino, S. Bordiga, Chem. Mater. 20 (2008) 4957.
[168] S. Chavan, J.G. Vitillo, E. Groppo, F. Bonino, C. Lamberti, P.D.C. Dietzel, S. Bordiga, J. Phys. Chem. C 113 (2009) 3292.
[169] S. Chavan, F. Bonino, J.G. Vitillo, E. Groppo, C. Lamberti, P.D.C. Dietzel, A. Zecchina, S. Bordiga, Phys. Chem. Chem. Phys. 11 (2009) 9811.
[170] G.P. Diakun, Nature 344 (1990) 83.
[171] H.H. Thorp, Inorg. Chem. 31 (1992) 1585.
[172] W.T. Liu, H.H. Thorp, Inorg. Chem. 32 (1993) 4102.
[173] R.W. Strange, M. Ellis, S.S. Hasnain, Coord. Chem. Rev. 249 (2005) 197.
[174] B.J. Gaffney, Annu. Rev. Biophys. Biomolec. Struct. 25 (1996) 431.
[175] F. Boffi, I. Ascone, S. Della Longa, M. Girasole, G. Yalovega, A.V. Soldatov, A. Varoli-Piazza, A.C. Castellano, Eur. Biophys. J. Biophys. Lett. 32 (2003) 329.
[176] J. Chan, M.E. Merrifield, A.V. Soldatov, M.J. Stillman, Inorg. Chem. 44 (2005) 4923.
[177] J. Yano, J. Kern, K.D. Irrgang, M.J. Latimer, U. Bergmann, P. Glatzel, Y. Pushkar, J. Biesiadka, B. Loll, K. Sauer, J. Messinger, A. Zouni, V.K. Yachandra, Proc. Natl. Acad. Sci. USA 102 (2005) 12047.
[178] A. Arcovito, M. Benfatto, M. Cianci, S.S. Hasnain, K. Nienhaus, G.U. Nienhaus, C. Savino, R.W. Strange, B. Vallone, S. Della Longa, Proc. Natl. Acad. Sci. USA 104 (2007) 6211.
[179] A. Arcovito, T. Moschetti, P. D'Angelo, G. Mancini, B. Vallone, M. Brunori, S. Della Longa, Arch. Biochem. Biophys. 475 (2008) 7.
[180] P. D'Angelo, A. Lapi, V. Migliorati, A. Arcovito, M. Benfatto, O.M. Roscioni, W. Meyer-Klaucke, S. Della-Longa, Inorg. Chem. 47 (2008) 9905.
[181] P. D'Angelo, S. Della Longa, A. Arcovito, M. Anselmi, A. Di Nola, G. Chillemi, J. Am. Chem. Soc. 132 (2010) 14901.
[182] J.J.H. Cotelesage, M.J. Pushie, P. Grochulski, I.J. Pickering, G.N. George, J. Inorg. Biochem. 115 (2012) 127.
[183] J. Kowalska, S. DeBeer, Biochim. Biophys. Acta-Mol. Cell Res. 1853 (2015) 1406.
[184] R. Le Toquin, W. Paulus, A. Cousson, C. Prestipino, C. Lamberti, J. Am. Chem. Soc. 128 (2006) 13161.
[185] A. Piovano, G. Agostini, A.I. Frenkel, T. Bertier, C. Prestipino, M. Ceretti, W. Paulus, C. Lamberti, J. Phys. Chem. C 115 (2011) 1311.
[186] J. García, G. Subías, J. Blasco, XAS Studies on Mixed Valence Oxides, in: J.A. van Bokhoven, C. Lamberti (Eds.), X-Ray Absorption and X-Ray Emission Spectroscopy: Theory and Applications, John Wiley & Sons, Chichester (UK), 2016, p. 459.
[187] J.C. Mikkelsen, J.B. Boyce, Phys. Rev. Lett. 49 (1982) 1412.
[188] C. Lamberti, S. Bordiga, F. Boscherini, S. Pascarelli, G.M. Schiavini, Appl. Phys. Lett. 64 (1994) 1430.
[189] S. Pascarelli, F. Boscherini, C. Lamberti, S. Mobilio, Phys. Rev. B 56 (1997) 1936.
[190] C. Lamberti, S. Bordiga, F. Boscherini, S. Mobilio, S. Pascarelli, L. Gastaldi, M. Madella, C. Papuzza, C. Rigo, D. Soldani, C. Ferrari, L. Lazzarini, G. Salviati, J. Appl. Phys. 83 (1998) 1058.
[191] F. Boscherini, C. Lamberti, S. Pascarelli, C. Rigo, S. Mobilio, Phys. Rev. B 58 (1998) 10745.
[192] F. Romanato, D. De Salvador, M. Berti, A. Drigo, M. Natali, M. Tormen, G. Rossetto, S. Pascarelli, F. Boscherini, C. Lamberti, S. Mobilio, Phys. Rev. B 57 (1998) 14619.
[193] L. Mino, D. Gianolio, G. Agostini, A. Piovano, M. Truccato, A. Agostino, S. Cagliero, G. Martinez-Criado, F. d'Acapito, S. Codato, C. Lamberti, Small 7 (2011) 930.
[194] F. Boscherini, X-ray absorption fine structure in the study of semiconductor heterostructures and nanostructures, in: C. Lamberti, G. Agostini (Eds.), Characterization of Semiconductor Heterostructures and Nanostructures (2nd Edition), Elsevier, Amsterdam, 2013, p. 259.
[195] M. Benfatto, A. Congiu-Castellano, A. Daniele, S.D. Longa, J. Synchrotron Radiat. 8 (2001) 267.
[196] M. Benfatto, S. Della Longa, C.R. Natoli, J. Synchrotron Radiat. 10 (2003) 51.
[197] M. Benfatto, S. Della Longa, J. Phys. Conf. Ser. 190 (2009) 012145.
[198] J.J. Rehr, A.L. Ankudinov, Coord. Chem. Rev. 249 (2005) 131.
[199] Y. Joly, S. Grenier, Theory of X-Ray Absorption Near Edge Structure, in: J.A. van Bokhoven, C. Lamberti (Eds.), X-Ray Absorption and X-Ray Emission Spectroscopy: Theory and Applications, John Wiley & Sons, Chichester (UK), 2016, p. 73.
[200] D. Gianolio, E. Groppo, J.G. Vitillo, A. Damin, S. Bordiga, A. Zecchina, C. Lamberti, Chem. Commun. 46 (2010) 976.
[201] E. Borfecchia, S. Maurelli, D. Gianolio, E. Groppo, M. Chiesa, F. Bonino, C. Lamberti, J. Phys, Chem. C 116 (2012) 19839.
[202] S.A. Guda, A.A. Guda, M.A. Soldatov, K.A. Lomachenko, A.L. Bugaev, C. Lamberti, W. Gawelda, C. Bressler, G. Smolentsev, A.V. Soldatov, Y. Joly, J. Chem. Theory Comput. 11 (2015) 4512.
[203] Y. Tulchinsky, C.H. Hendon, K.A. Lomachenko, E. Borfecchia, B.C. Melot, M.R. Hudson, J.D. Tarver, M.D. Korzynski, A.W. Stubbs, J.J. Kagan, C. Lamberti, C.M. Brown, M. Dinca, J. Am. Chem. Soc 139 (2017) 5992.
[204] C. Barzan, A. Piovano, L. Braglia, G.A. Martino, C. Lamberti, S. Bordiga, E. Groppo, J. Am. Chem. Soc. 139 (2017) 17064.
[205] G. Bunker, Introduction to XAFS: A Practical Guide to X-ray Absorption Fine Structure Spectroscopy, Cambridge University Press, Cambridge, 2010.
[206] S. Calvin, XAFS for Everyone, Taylor & Francis, 2013.
[207] P. Willmott, An Introduction to Synchrotron Radiation: Techniques and Applications, Wiley, Singapore, 2011.
[208] M. Nachtegaal, O. Müller, C. König, R. Frahm, QEXAFS: Techniques and Scientific Applications for Time-Resolved XAS, in: J.A. van Bokhoven, C. Lamberti (Eds.), X-Ray Absorption and X-Ray Emission Spectroscopy: Theory and Applications, John Wiley & Sons, Chichester (UK), 2016, p. 155.
[209] O. Mathon, I. Kantor, S. Pascarelli, Time-Resolved XAS Using an Energy Dispersive Spectrometer: Techniques and Applications, in: J.A. van Bokhoven, C. Lamberti (Eds.), X-Ray Absorption and X-Ray Emission Spectroscopy: Theory and Applications, John Wiley & Sons, Chichester (UK), 2016, p. 185.
[210] E. Borfecchia, C. Garino, L. Salassa, C. Lamberti, Philos. Trans. R. Soc. Math. Phys. Eng. Sci. 371 (2013).
[211] G. Martinez-Criado, B. Borfecchia, L. Mino, C. Lamberti, Micro- and nano-X-ray beams, in: C. Lamberti, G. Agostini (Eds.), Characterization of Semiconductor Heterostructures and Nanostructures (2nd Edition), Elsevier, Amsterdam, 2013, p. 361.
[212] L. Mino, E. Borfecchia, J. Segura-Ruiz, C. Giannini, G. Martinez-Criado, C. Lamberti, Rev. Mod. Phys. 90 (2018) 025007.
[213] J.-P. Itié, F. Baudelet, J.-P. Rueff, High Pressure XAS, XMCD and IXS, in: J.A. van Bokhoven, C. Lamberti (Eds.), X-Ray Absorption and X-Ray Emission Spectroscopy: Theory and Applications, John Wiley & Sons, Chichester (UK), 2016, p. 385.
[214] F. Farges, M. Cotte, X-Ray Absorption Spectroscopy and Cultural Heritage: Highlights and Perspectives, in: J.A. van Bokhoven, C. Lamberti (Eds.), X-Ray Absorption and X-Ray Emission Spectroscopy: Theory and Applications, John Wiley & Sons, Chichester (UK), 2016, p. 609.
[215] M.A. Denecke, X-ray spectroscopy in studies of the nuclear fuel cycle, in: J.A. van Bokhoven, C. Lamberti (Eds.), X-Ray Absorption and X-Ray Emission Spectroscopy: Theory and Applications, John Wiley & Sons, Chichester (UK), 2016, p. 523.
[216] D. Gianolio, How to start an XAS experiment, in: J.A. van Bokhoven, C. Lamberti (Eds.), X-Ray Absorption and X-Ray Emission Spectroscopy: Theory and Applications, John Wiley & Sons, Chichester (UK), 2016, p. 99.
[217] J. Stöhr, NEXAFS spectroscopy, Springer, Berlin Heidelberg, Berlin, 2013.
[218] J.A. van Bokhoven, T. Ressler, F.M.F. de Groot, G. Knopp-Gericke, Extended X-ray absorption fine structure spectroscopy, in: H.S. Nalwa (Ed.), In-situ Spectroscopy of Catalysts, American Scientific Publishers, 2004.
[219] F.M.F. de Groot, A. Knop-Gericke, T. Ressler, J.A. van Bokhoven, X-ray absorption near edge spectroscopy, in: H.S. Nalwa (Ed.), In-situ spectroscopy of catalysts, American Scientific Publishers, 2004.
[220] D.E. Sayers, E.A. Stern, F.W. Lytle, Phys. Rev. Lett. 27 (1971) 1204.
[221] E.A. Stern, S.M. Heald, E. Koch, Handb. Synchrotron Radiat. (1983).
[222] A. Filipponi, J. Phys. Condes. Matter 13 (2001) R23.
[223] G. Agostini, S. Usseglio, E. Groppo, M.J. Uddin, C. Prestipino, S. Bordiga, A. Zecchina, P.L. Solari, C. Lamberti, Chem. Mater. 21 (2009) 1343.
[224] G. Agostini, R. Pellegrini, G. Leofanti, L. Bertinetti, S. Bertarione, E. Groppo, A. Zecchina, C. Lamberti, J. Phys. Chem. C 113 (2009) 10485.
[225] R. Pellegrini, G. Agostini, E. Groppo, A. Piovano, G. Leofanti, C. Lamberti, J. Catal. 280 (2011) 150.
[226] M.L. Neidig, J. Sharma, H.C. Yeh, J.S. Martinez, S.D. Conradson, A.P. Shreve, J. Am. Chem. Soc 133 (2011) (1839) 11837.
[227] A.V. Soldatov, K.A. Lomachenko, Nanostructured materials, in: J.A. van Bokhoven, C. Lamberti (Eds.), X-Ray Absorption and X-Ray Emission Spectroscopy: Theory and Applications, John Wiley & Sons, Chichester (UK), 2016, p. 809.
[228] C. Lamberti, Surf. Sci. Rep. 53 (2004) 1.
[229] M.S. Seehra, P. Dutta, S. Neeleshwar, Y.Y. Chen, C.L. Chen, S.W. Chou, C.C. Chen, C.L. Dong, C.L. Chang, Adv. Mater. 20 (2008) 1656.

[230] A.M. Jawaid, S. Chattopadhyay, D.J. Wink, L.E. Page, P.T. Snee, Acs Nano 7 (2013) 3190.
[231] J.W. Lee, D.Y. Son, T.K. Ahn, H.W. Shin, I.Y. Kim, S.J. Hwang, M.J. Ko, S. Sul, H. Han, N.G. Park, Sci. Rep. 3 (2013) 1050.
[232] V. Srivastava, W.Y. Liu, E.M. Janke, V. Kamysbayev, A.S. Filatov, C.J. Sun, B. Lee, T. Rajh, R.D. Schaller, D.V. Talapin, Nano Lett. 17 (2017) 2094.
[233] A.A. Guda, S. M.A., S. A.V., Group III-V and II-VI Quantum Dots, in: C.S. Schnohr, M.C. Ridgway (Eds.), X-Ray Absorption Spectroscopy of Semiconductors, Springer, Heidelberg, 2016.
[234] E. Groppo, C. Prestipino, C. Lamberti, P. Luches, C. Giovanardi, F. Boscherini, J. Phys. Chem. B 107 (2003) 4597.
[235] C. Lamberti, E. Groppo, C. Prestipino, S. Casassa, A.M. Ferrari, C. Pisani, C. Giovanardi, P. Luches, S. Valeri, F. Boscherini, Phys. Rev. Lett. 91 (2003) 4.
[236] E. Groppo, C. Prestipino, C. Lamberti, R. Carboni, F. Boscherini, P. Luches, S. Valeri, S. D'Addato, Phys. Rev. B 70 (2004) 6.
[237] P. Luches, S. D'Addato, S. Valeri, E. Groppo, C. Prestipino, C. Lamberti, F. Boscherini, Phys. Rev. B 69 (2004) 9.
[238] Q.H. Liu, W.S. Yan, H. Wei, Z.H. Sun, Z.Y. Pan, A.V. Soldatov, C. Mai, C.J. Pei, X.F. Zhang, Y. Jiang, S.Q. Wei, Phys. Rev. B 77 (2008).
[239] S. Bordiga, S. Coluccia, C. Lamberti, L. Marchese, A. Zecchina, F. Boscherini, F. Buffa, F. Genoni, G. Leofanti, G. Petrini, G. Vlaic, J. Phys. Chem. 98 (1994) 4125.
[240] S. Bordiga, F. Bonino, A. Damin, C. Lamberti, Phys. Chem. Chem. Phys. 9 (2007) 4854.
[241] G. Ricchiardi, A. Damin, S. Bordiga, C. Lamberti, G. Spanò, F. Rivetti, A. Zecchina, J. Am. Chem. Soc. 123 (2001) 11409.
[242] J.A. van Bokhoven, C. Lamberti, Coord. Chem. Rev. 277 (2014) 275.
[243] S.J. Gurman, N. Binsted, I. Ross, J. Phys. C-Solid State Phys. 19 (1986) 1845.
[244] L. Fonda, J. Phys. Condensed Matter 4 (1992) 8269.
[245] J.J. Rehr, R.C. Albers, S.I. Zabinsky, Phys. Rev. Lett. 69 (1992) 3397.
[246] A. Filipponi, A. Di Cicco, T.A. Tyson, C.R. Natoli, Solid State Commun. 78 (1991) 265.
[247] A. Filipponi, A. Di Cicco, Phys. Rev. B 52 (1995) 15135.
[248] A. Frenkel, E.A. Stern, A. Voronel, M. Qian, M. Newville, Phys. Rev. B 49 (1994) 11662.
[249] M.S. Nashner, A.I. Frenkel, D.L. Adler, J.R. Shapley, R.G. Nuzzo, J. Am. Chem. Soc. 119 (1997) 7760.
[250] A.I. Frenkel, J. Synchrotron Radiat. 6 (1999) 293.
[251] A.I. Frenkel, A. Yevick, C. Cooper, R. Vasic, Modeling the Structure and Composition of Nanoparticles by Extended X-Ray Absorption Fine-Structure Spectroscopy, in: R.G. Cooks, E.S. Yeung (eds.) Annual Review of Analytical Chemistry, Vol 4, Annual Reviews, Palo Alto, 2011, pp. 23–39.
[252] N. Binsted, S.L. Cook, J. Evans, G.N. Greaves, R.J. Price, J. Am. Chem. Soc. 109 (1987) 3669.
[253] S. Kawi, J.R. Chang, B.C. Gates, J. Am. Chem. Soc. 115 (1993) 4830.
[254] O. Alexeev, B.C. Gates, Top. Catal. 10 (2000) 273.
[255] C. Lamberti, G.T. Palomino, S. Bordiga, G. Berlier, F. D'Acapito, A. Zecchina, Angew. Chem., Int. Edit. 39 (2000) 2138.
[256] C. Prestipino, L. Capello, F. D'Acapito, C. Lamberti, Phys. Chem. Chem. Phys. 7 (2005) 1743.
[257] D. Yang, S.O. Odoh, J. Borycz, T.C. Wang, O.K. Farha, J.T. Hupp, C.J. Cramer, L. Gagliardi, B.C. Gates, ACS Catal. 6 (2016) 235.
[258] C. Tyrsted, E. Borfecchia, G. Berlier, K.A. Lomachenko, C. Lamberti, S. Bordiga, P.N.R. Vennestrom, T.V.W. Janssens, H. Falsig, P. Beato, A. Puig-Molina, Catal. Sci. Technol. 6 (2016) 8314.
[259] C. Lamberti, C. Prestipino, F. Bonino, L. Capello, S. Bordiga, G. Spoto, A. Zecchina, S.D. Moreno, B. Cremaschi, M. Garilli, A. Marsella, D. Carmello, S. Vidotto, G. Leofanti, Angew. Chem., Int. Edit. 41 (2002) 2341.
[260] E. Groppo, M.J. Uddin, S. Bordiga, A. Zecchina, C. Lamberti, Angew. Chem., Int. Edit. 47 (2008) 9269.
[261] N.B. Muddada, U. Olsbye, L. Caccialupi, F. Cavani, G. Leofanti, D. Gianolio, S. Bordiga, C. Lamberti, Phys. Chem. Chem. Phys. 12 (2010) 5605.
[262] K.A. Lomachenko, E. Borfecchia, C. Negri, G. Berlier, C. Lamberti, P. Beato, H. Falsig, S. Bordiga, J. Am. Chem. Soc 138 (2016) 12025.
[263] C.W. Andersen, E. Borfecchia, M. Bremholm, M.R.V. Jorgensen, P.N.R. Vennestrom, C. Lamberti, L.F. Lundegaard, B.B. Iversen, Angew. Chem., Int. Edit. 56 (2017) 10367.
[264] D.K. Pappas, E. Borfecchia, M. Dyballa, I.A. Pankin, K.A. Lomachenko, A. Martini, M. Signorile, S. Teketel, B. Arstad, G. Berlier, C. Lamberti, S. Bordiga, U. Olsbye, K.P. Lillerud, S. Svelle, P. Beato, J. Am. Chem. Soc. 139 (2017) 14961.
[265] A.W. Stubbs, L. Braglia, E. Borfecchia, R.J. Meyer, Y. Roman-Leshkov, C. Lamberti, M. Dinca, ACS Catal. 8 (2018) 596.
[266] A. Bianconi, M. Dell'Ariccia, A. Gargano, C.R. Natoli, Bond Length Determination Using XANES, in: A. Bianconi, L. Incoccia, S. Stipcich (eds.) EXAFS and Near Edge Structure: Proceedings of the International Conference Frascati, Italy, September 13–17, 1982, Springer Berlin Heidelberg, Berlin, Heidelberg, 1983, pp. 57–61.
[267] C.R. Natoli, Distance dependence of continuum and bound state of excitonic resonances in X-Ray Absorption Near Edge Structure (XANES), in: K.O. Hodgson, B. Hedman, J.E. Penner-Hahn (Eds.), EXAFS and Near Edge Structure III, Springer Series in Chemical Physics, 2, Springer, Berlin, 1984, p. 38.
[268] K.A. Lomachenko, E. Borfecchia, S. Bordiga, A.V. Soldatov, P. Beato, C. Lamberti, J. Phys. Conf. Series 712 (2016) 012041.
[269] I.A. Pankin, A.A. Guda, N.A. Tumanov, Y. Filinchuk, K.A. Lomachenko, A.L. Bugaev, S.A. Guda, V.V. Shapovalov, C. Lamberti, A.V. Soldatov, J. Alloys Compounds 735 (2018) 277.
[270] M.A. Soldatov, J. Gottlicher, S.P. Kubrin, A.A. Guda, T.A. Lastovina, A.L. Bugaev, Y.V. Rusalev, A.V. Soldatov, C. Lamberti, J. Phys. Chem. C 122 (2018) 8543.
[271] A.I. Frenkel, Chem. Soc. Rev. 41 (2012) 8163.
[272] J. Yano, V.K. Yachandra, Photosynthesis Res. 102 (2009) 241.
[273] G. Smolentsev, A.V. Soldatov, Comput. Mater. Sci. 39 (2007) 569.
[274] J.J. Rehr, J.J. Kas, M.P. Prange, A.P. Sorini, Y. Takimoto, F. Vila, Comptes Rendus Phys. 10 (2009) 548.
[275] J.J. Rehr, J.J. Kas, F.D. Vila, M.P. Prange, K. Jorissen, Phys. Chem. Chem. Phys. 12 (2010) 5503.
[276] A. Bianconi, J. Garcia, M. Benfatto, A. Marcelli, C.R. Natoli, M.F. Ruiz-Lopez, Phys. Rev. B 43 (1991) 6885.
[277] T.A. Tyson, K.O. Hodgson, C.R. Natoli, M. Benfatto, Phys. Rev. B 46 (1992) 5997.
[278] Y. Joly, Phys. Rev. B 63 (2001).
[279] Y. Joly, J. Synchrotron Radiat. 10 (2003) 58.
[280] H. Ebert, Fully relativistic band structure calculations for magnetic solids – formalism and application, in: H. Dreyssé (Ed.), Electronic Structure and Physical Properties of Solids: the Users of the LMTO method, Springer, Berlin, 2000, p. 191.
[281] H. Ebert, D. Kodderitzsch, J. Minar, Rep. Prog. Phys. 74 (2011) 096501.
[282] S. Della Longa, A. Arcovito, M. Girasole, J.L. Hazemann, M. Benfatto, Phys. Rev. Lett. 87 (2001) 155501.
[283] V.N. Datsyuk, Gegusin II, R.V. Vedrinskii, Phys. Status Solidi B-Basic Res. 134 (1986) 175.
[284] R.V. Vedrinskii, I.I. Gegusin, V.N. Datsyuk, A.A. Novakovich, V.L. Kraizman, Phys. Status Solidi B 111 (1982) 433.
[285] G. te Velde, F.M. Bickelhaupt, E.J. Baerends, C.F. Guerra, S.J.A. Van Gisbergen, J. G. Snijders, T. Ziegler, J. Comput. Chem. 22 (2001) 931.
[286] F. Neese, Wiley Interdiscip Rev.-Comput. Mol. Sci. 2 (2012) 73.
[287] F. Neese, Wiley Interdiscip Rev. Comput. Mol. Sci. 8 (2018) e1327.
[288] K. Schwarz, P. Blaha, G.K.H. Madsen, Comput. Phys. Commun. 147 (2002) 71.
[289] K. Schwarz, P. Blaha, Comput. Mater. Sci. 28 (2003) 259.
[290] K. Schwarz, P. Blaha, S.B. Trickey, Mol. Phys. 108 (2010) 3147.
[291] P. Giannozzi, S. Baroni, N. Bonini, M. Calandra, R. Car, C. Cavazzoni, D. Ceresoli, G.L. Chiarotti, M. Cococcioni, I. Dabo, A. Dal Corso, S. de Gironcoli, S. Fabris, G. Fratesi, R. Gebauer, U. Gerstmann, C. Gougoussis, A. Kokalj, M. Lazzeri, L. Martin-Samos, N. Marzari, F. Mauri, R. Mazzarello, S. Paolini, A. Pasquarello, L. Paulatto, C. Sbraccia, S. Scandolo, G. Sclauzero, A.P. Seitsonen, A. Smogunov, P. Umari, R.M. Wentzcovitch, J. Phys. Condens. Matter 21 (2009) 395502.
[292] P. Giannozzi, O. Andreussi, T. Brumme, O. Bunau, M.B. Nardelli, M. Calandra, R. Car, C. Cavazzoni, D. Ceresoli, M. Cococcioni, N. Colonna, I. Carnimeo, A. Dal Corso, S. de Gironcoli, P. Delugas, R.A. DiStasio, A. Ferretti, A. Floris, G. Fratesi, G. Fugallo, R. Gebauer, U. Gerstmann, F. Giustino, T. Gorni, J. Jia, M. Kawamura, H.Y. Ko, A. Kokalj, E. Kucukbenli, M. Lazzeri, M. Marsili, N. Marzari, F. Mauri, N.L. Nguyen, H.V. Nguyen, A. Otero-de-la-Roza, L. Paulatto, S. Ponce, D. Rocca, R. Sabatini, B. Santra, M. Schlipf, A.P. Seitsonen, A. Smogunov, I. Timrov, T. Thonhauser, P. Umari, N. Vast, X. Wu, S. Baroni, J. Phys. Condens. Matter 29 (2017) 465901.
[293] P. Giannozzi, C. Cavazzoni, Nuovo Cimento Soc. Ital. Fis. C-Colloq. Phys. 32 (2009) 49.
[294] M. Taillefumier, D. Cabaret, A.-M. Flank, F. Mauri, Phys. Rev. B 66 (2002) 195107.
[295] M.W. Haverkort, M. Zwierzycki, O.K. Andersen, Phys. Rev. B 85 (2012) 165113.
[296] A. Tanaka, T. Jo, J. Phys. Soc. Jpn. 63 (1994) 2788.
[297] E. Stavitski, F.M.F. de Groot, Micron 41 (2010) 687.
[298] J. Vinson, J.J. Rehr, J.J. Kas, E.L. Shirley, Phys. Rev. B 83 (2011) 115106.
[299] K. Gilmore, J. Vinson, E.L. Shirley, D. Prendergast, C.D. Pemmaraju, J.J. Kas, F.D. Vila, J.J. Rehr, Comput. Phys. Commun. 197 (2015) 109.
[300] S. Sagmeister, C. Ambrosch-Draxl, Phys. Chem. Chem. Phys. 11 (2009) 4451.
[301] D. Nabok, A. Gulans, C. Draxl, Phys. Rev. B 94 (2016) 035118.
[302] G. Karlstrom, R. Lindh, P.A. Malmqvist, B.O. Roos, U. Ryde, V. Veryazov, P.O. Widmark, M. Cossi, B. Schimmelpfennig, P. Neogrady, L. Seijo, Comput. Mater. Sci. 28 (2003) 222.
[303] K. Jorissen, F.D. Vila, J.J. Rehr, Comput. Phys. Commun. 183 (2012) 1911.
[304] K. Jorissen, J.J. Rehr, New Developments in FEFF: FEFF9 and JFEFF, in: Z.Y. Wu (Ed.) 15th International Conference on X-Ray Absorption Fine Structure, 2013.
[305] C.R. Natoli, M. Benfatto, S. Doniach, Phys. Rev. A 34 (1986) 4682.
[306] G. Smolentsev, G. Guilera, M. Tromp, S. Pascarelli, A.V. Soldatov, J. Chem. Phys. 130 (2009) 174508.
[307] G. Smolentsev, A. Soldatov, J. Synchrotron Radiat. 13 (2005) 19.
[308] A.L. Bugaev, O.A. Usoltsev, A.A. Guda, K.A. Lomachenko, I.A. Pankin, Y.V. Rusalev, H. Emerich, E. Groppo, R. Pellegrini, A.V. Soldatov, J.A. van Bokhoven, C. Lamberti, J. Phys. Chem. C 122 (2018) 12029.
[309] A.L. Bugaev, O.A. Usoltsev, A. Lazzarini, K.A. Lomachenko, A.A. Guda, R. Pellegrini, M. Carosso, J.G. Vitillo, E. Groppo, J. van Bokhoven, A.V. Soldatov, C. Lamberti, Faraday Discuss 208 (2018) 187.
[310] F.W. Lytle, D.E. Sayers, E.A. Stern, Phys. Rev. B 11 (1975) 4825.
[311] E.A. Stern, Phys. Rev. B 10 (1974) 3027.
[312] J.J. Kas, A.P. Sorini, M.P. Prange, L.W. Cambell, J.A. Soininen, J.J. Rehr, Phys. Rev. B 76 (2007), Art. n. 195116.
[313] B.K. Teo, P.A. Lee, J. Am. Chem. Soc. 101 (1979) 2815.
[314] A.G. McKale, B.W. Veal, A.P. Paulikas, S.K. Chan, G.S. Knapp, J. Am. Chem. Soc. 110 (1988) 3763.

[315] Y. Iwasawa, X-ray absorption fine structure for catalysts and surfaces, Iwasawa, Y. ed., World Scientific, 1996.
[316] X.G. Shao, L.M. Shao, G.W. Zhao, Anal. Commun. 35 (1998) 135.
[317] Y. Koichiro, I. Yoshiaki, M. Takeshi, T. Masao, E. Shuichi, Phys. Rev. B 32 (1999) 1393.
[318] M. Munoz, P. Argoul, F. Farges, Am. Miner. 88 (2003) 694.
[319] H. Funke, A.C. Scheinost, M. Chukalina, Phys. Rev. B 71 (2005) 7.
[320] T.J. Penfold, I. Tavernelli, C.J. Milne, M. Reinhard, A. El Nahhas, R. Abela, U. Rothlisberger, M. Chergui, J. Chem. Phys. 138 (2013) 7.
[321] J. Timoshenko, A. Kuzmin, Comput. Phys. Commun. 180 (2009) 920.
[322] C.K. Chui, An introduction to wavelets, Academic Press, 1992.
[323] P. Argoul, T.P. Le, Wavelet analysis of transient signals in civil engineering, in: F. M., M. F. (Ed.), Novel Approaches in Civil Engineering, Springer, Berlin, Heidelberg, 2004, p. 311.
[324] L. Valenzano, J.G. Vitillo, S. Chavan, B. Civalleri, F. Bonino, S. Bordiga, C. Lamberti, Catal. Today 182 (2012) 67.
[325] E. Gallo, E. Gorelov, A.A. Guda, A.L. Bugaev, F. Bonino, E. Borfecchia, G. Ricchiardi, D. Gianolio, S. Chavan, C. Lamberti, Inorg. Chem. 56 (2017) 14408.
[326] S.L. Qiu, G.S. Zhu, Coord. Chem. Rev. 253 (2009) 2891.
[327] Z. Wang, S.M. Cohen, Chem. Soc. Rev. 38 (2009) 1315.
[328] S. Chavan, J.G. Vitillo, M.J. Uddin, F. Bonino, C. Lamberti, E. Groppo, K.P. Lillerud, S. Bordiga, Chem. Mater. 22 (2010) 4602.
[329] H.X. Deng, C.J. Doonan, H. Furukawa, R.B. Ferreira, J. Towne, C.B. Knobler, B. Wang, O.M. Yaghi, Science 327 (2010) 846.
[330] B.L. Chen, S.C. Xiang, G.D. Qian, Acc. Chem. Res. 43 (2010) 1115.
[331] K.K. Tanabe, S.M. Cohen, Chem. Soc. Rev. 40 (2011) 498.
[332] S.M. Cohen, Chem. Rev. 112 (2012) 970.
[333] N.C. Thacker, P. Ji, Z. Lin, A. Urban, W. Lin, Faraday Discuss 201 (2017) 303.
[334] M.I. Gonzalez, J. Oktawiec, J.R. Long, Faraday Discuss 201 (2017) 351.
[335] T. Toyao, K. Miyahara, M. Fujiwaki, T.H. Kim, S. Dohshi, Y. Horiuchi, M. Matsuoka, J. Phys. Chem. C 119 (2015) 8131.
[336] L. Braglia, E. Borfecchia, L. Maddalena, S. Øien, K.A. Lomachenko, A.L. Bugaev, S. Bordiga, A.V. Soldatov, K.P. Lillerud, C. Lamberti, Catal. Today 283 (2017) 89.
[337] L. Braglia, E. Borfecchia, K.A. Lomachenko, A.L. Bugaev, A.A. Guda, A.V. Soldatov, B.T.L. Bleken, S. Oien, U. Olsbye, K.P. Lillerud, S. Bordiga, G. Agostini, M. Manzoli, C. Lamberti, Faraday Discuss 201 (2017) 265.
[338] C.H. Hendon, J. Bonnefoy, E.A. Quadrelli, J. Canivet, M.B. Chambers, G. Rousse, A. Walsh, M. Fontecave, C. Mellot-Draznieks, Chem. Eur. J. 22 (2016) 3713.
[339] L. Braglia, E. Borfecchia, K. Lomachenko, S. Øien, K. Lillerud, C. Lamberti, J. Phys. Conf. Ser. 712 (2016) 012053.
[340] S. Øien, G. Agostini, S. Svelle, E. Borfecchia, K.A. Lomachenko, L. Mino, E. Gallo, S. Bordiga, U. Olsbye, K.P. Lillerud, C. Lamberti, Chem. Mater. 27 (2015) 1042.
[341] T. Toyao, M. Saito, S. Dohshi, K. Mochizuki, M. Iwata, H. Higashimura, Y. Horiuchi, M. Matsuoka, Res. Chem. Intermed. 42 (2016) 7679.
[342] E. Borfecchia, S. Øien, S. Svelle, L. Mino, L. Braglia, G. Agostini, E. Gallo, K. Lomachenko, S. Bordiga, A. Guda, S.M. A., A.V. Soldatov, U. Olsbye, K.P. Lillerud, C. Lamberti, J. Phys. Conf. Ser. 712 (2016) 012125.
[343] L. Braglia, E. Borfecchia, A. Martini, A.L. Bugaev, A.V. Soldatov, S. Oien-Odegaard, B.T. Lonstad-Bleken, U. Olsbye, K.P. Lillerud, K.A. Lomachenko, G. Agostini, M. Manzoli, C. Lamberti, Phys. Chem. Chem. Phys. 19 (2017) 27489.
[344] H.H. Fei, S.M. Cohen, Chem. Commun. 50 (2014) 4810.
[345] L.Y. Chen, X.D. Chen, H.L. Liu, C.H. Bai, Y.W. Li, J. Mater. Chem. A 3 (2015) 15259.
[346] A.L. Bugaev, A.A. Guda, K.A. Lomachenko, E.G. Kamyshova, M.A. Soldatov, G. Kaur, S. Øien-Ødegaard, L. Braglia, A. Lazzarini, M. Manzoli, S. Bordiga, U. Olsbye, K.P. Lillerud, A.V. Soldatov, C. Lamberti, Faraday Discuss 208 (2018) 287.
[347] A.L. Bugaev, A.A. Guda, A. Lazzarini, K.A. Lomachenko, E. Groppo, R. Pellegrini, A. Piovano, H. Emerich, A.V. Soldatov, L.A. Bugaev, V.P. Dmitriev, J.A. van Bokhoven, C. Lamberti, Catal. Today 283 (2017) 119.
[348] P.Q. Yin, T. Yao, Y. Wu, L.R. Zheng, Y. Lin, W. Liu, H.X. Ju, J.F. Zhu, X. Hong, Z.X. Deng, G. Zhou, S.Q. Wei, Y.D. Li, Angew. Chem., Int. Edit. 55 (2016) 10800.
[349] Y.J. Chen, S.F. Ji, Y.G. Wang, J.C. Dong, W.X. Chen, Z. Li, R.A. Shen, L.R. Zheng, Z. B. Zhuang, D.S. Wang, Y.D. Li, Angew. Chem., Int. Edit. 56 (2017) 6937.
[350] T. He, S.M. Chen, B. Ni, Y. Gong, Z. Wu, L. Song, L. Gu, W.P. Hu, X. Wang, Angew. Chem., Int. Edit. 57 (2018) 3493.
[351] W. Chen, J. Pei, C.-T. He, J. Wan, H. Ren, Y. Wang, J. Dong, K. Wu, W.-C. Cheong, J. Mao, X. Zheng, W. Yan, Z. Zhuang, C. Chen, Q. Peng, D. Wang, Y. Li, Adv. Mater. 30 (2018) 1800396.
[352] S.L. Zhao, Y. Wang, J.C. Dong, C.T. He, H.J. Yin, P.F. An, K. Zhao, X.F. Zhang, C. Gao, L.J. Zhang, J.W. Lv, J.X. Wang, J.Q. Zhang, A.M. Khattak, N.A. Khan, Z.X. Wei, J. Zhang, S.Q. Liu, H.J. Zhao, Z.Y. Tang, Nat. Energy 1 (2016) 1.
[353] X. Wang, W.X. Chen, L. Zhang, T. Yao, W. Liu, Y. Lin, H.X. Ju, J.C. Dong, L.R. Zheng, W.S. Yan, X.S. Zheng, Z.J. Li, X.Q. Wang, J. Yang, D.S. He, Y. Wang, Z.X. Deng, Y.E. Wu, Y.D. Li, J. Am. Chem. Soc. 139 (2017) 9419.
[354] C. Bianchini, V. Dal Santo, A. Meli, S. Moneti, M. Moreno, W. Oberhauser, R. Psaro, L. Sordelli, F. Vizza, Angew. Chem., Int. Edit. 42 (2003) 2636.
[355] M. Taoufik, E. Le Roux, J. Thivolle-Cazat, J.M. Basset, Angew. Chem., Int. Edit. 46 (2007) 7202.
[356] M. Rimoldi, D. Fodor, J.A. van Bokhoven, A. Mezzetti, Chem. Commun. 49 (2013) 11314.
[357] W.X. Gu, M.M. Stalzer, C.P. Nicholas, A. Bhattacharyya, A. Motta, J.R. Gallagher, G.H. Zhang, J.T. Miller, T. Kobayashi, M. Pruski, M. Delferro, T.J. Marks, J. Am. Chem. Soc. 137 (2015) 6770.
[358] R.J.C. Dubey, R.J. Comito, Z.W. Wu, G.H. Zhang, A.J. Rieth, C.H. Hendon, J.T. Miller, M. Dinca, J. Am. Chem. Soc. 139 (2017) 12664.
[359] G. Malta, S.J. Freakley, S.A. Kondrat, G.J. Hutchings, Chem. Commun. 53 (2017) 11733.
[360] T.Z.H. Gani, H.J. Kulik, ACS Catal. 8 (2018) 975.
[361] Sun Qi, Aguila Briana, Lyndsey D. Earl, Carter W. Abney, Wojtas Lukasz, Praveen K. Thallapally, Ma Shengqian, Adv. Mater. 30 (2018) 1705479.
[362] J. Timoshenko, K.R. Keller, A.I. Frenkel, J. Chem. Phys. 146 (2017).
[363] J. Lin, A.Q. Wang, B.T. Qiao, X.Y. Liu, X.F. Yang, X.D. Wang, J.X. Liang, J.X. Li, J.Y. Liu, T. Zhang, J. Am. Chem. Soc. 135 (2013) 15314.
[364] P.X. Liu, Y. Zhao, R.X. Qin, S.G. Mo, G.X. Chen, L. Gu, D.M. Chevrier, P. Zhang, Q. Guo, D.D. Zang, B.H. Wu, G. Fu, N.F. Zheng, Science 352 (2016) 797.
[365] H.B. Zhang, J. Wei, J.C. Dong, G.G. Liu, L. Shi, P.F. An, G.X. Zhao, J.T. Kong, X.J. Wang, X.G. Meng, J. Zhang, J.H. Ye, Angew. Chem., Int. Edit. 55 (2016) 14308.
[366] N. Kornienko, Y.B. Zhao, C.S. Kiley, C.H. Zhu, D. Kim, S. Lin, C.J. Chang, O.M. Yaghi, P.D. Yang, J. Am. Chem. Soc. 137 (2015) 14129.
[367] D.J. Darensbourg, W.C. Chung, K.C. Wang, H.C. Zhou, ACS Catal. 4 (2014) 1511.
[368] Y. An, Y.Y. Liu, P.F. An, J.C. Dong, B.Y. Xu, Y. Dai, X.Y. Qin, X.Y. Zhang, M.H. Whangbo, B.B. Huang, Angew. Chem., Int. Edit. 56 (2017) 3036.
[369] Z.J. Han, F. Qiu, R. Eisenberg, P.L. Holland, T.D. Krauss, Science 338 (2012) 1321.
[370] P. Jiang, Q. Liu, X.P. Sun, Nanoscale 6 (2014) 13440.
[371] T.T. Liu, A.M. Asiri, X.P. Sun, Nanoscale 8 (2016) 3911.
[372] Y. An, H.L. Li, Y.Y. Liu, B.B. Huang, Q.L. Sun, Y. Dai, X.Y. Qin, X.Y. Zhang, J. Solid State Chem. 233 (2016) 194.
[373] S.F. Ji, Y.J. Chen, Q. Fu, Y.F. Chen, J.C. Dong, W.X. Chen, Z. Li, Y. Wang, L. Gu, W. He, C. Chen, Q. Peng, Y. Huang, X.F. Duan, D.S. Wang, C. Draxl, Y.D. Li, J. Am. Chem. Soc. 139 (2017) 9795.
[374] X.L. Han, M.Y. Xu, S. Yang, J. Qian, D.B. Hua, J. Mater. Chem. A 5 (2017) 5123.
[375] B.Y. Li, Q. Sun, Y.M. Zhang, C.W. Abney, B. Aguila, W.B. Lin, S.Q. Ma, A.C.S. Appl, Mater. Interfaces 9 (2017) 12511.
[376] A.P. Cote, A.I. Benin, N.W. Ockwig, M. O'Keeffe, A.J. Matzger, O.M. Yaghi, Science 310 (2005) 1166.
[377] X. Feng, X.S. Ding, D.L. Jiang, Chem. Soc. Rev. 41 (2012) 6010.
[378] S.Y. Ding, W. Wang, Chem. Soc. Rev. 42 (2013) 548.
[379] J.L. Long, S.B. Wang, Z.X. Ding, S.C. Wang, Y.E. Zhou, L. Huang, X.X. Wang, Chem. Commun. 48 (2012) 11656.
[380] P.Y. Wu, C. He, J. Wang, X.J. Peng, X.Z. Li, Y.L. An, C.Y. Duan, J. Am. Chem. Soc 134 (2012) 14991.
[381] C.H. Hendon, D. Tiana, M. Fontecave, C. Sanchez, L. D'Arras, C. Sassoye, L. Rozes, C. Mellot-Draznieks, A. Walsh, J. Am. Chem. Soc 135 (2013) 10942.
[382] T. Toyao, M. Saito, Y. Horiuchi, K. Mochizuki, M. Iwata, H. Higashimura, M. Matsuoka, Catal. Sci. Technol. 3 (2013) 2092.
[383] C.F. Zhang, L.G. Qiu, F. Ke, Y.J. Zhu, Y.P. Yuan, G.S. Xu, X. Jiang, J. Mater. Chem. A 1 (2013) 14329.
[384] T. Toyao, M. Saito, S. Dohshi, K. Mochizuki, M. Iwata, H. Higashimura, Y. Horiuchi, M. Matsuoka, Chem. Commun. 50 (2014) 6779.
[385] K. Khaletskaya, A. Pougin, R. Medishetty, C. Rosler, C. Wiktor, J. Strunk, R.A. Fischer, Chem. Mater. 27 (2015) 7248.
[386] Z. Li, J.D. Xiao, H.L. Jiang, ACS Catal. 6 (2016) 5359.
[387] X.B. Yang, J. Chen, J.P. Hu, S.Y. Zhao, J.Y. Zhao, X.T. Luo, Catal. Sci. Technol. 8 (2018) 573.
[388] Y. Fang, Y. Ma, M. Zheng, P. Yang, A.M. Asiri, X. Wang, Coord. Chem. Rev. (2017).
[389] Q. Gao, J. Xu, X.-H. Bu, Coord. Chem. Rev. (2018).
[390] W.P. Lustig, S. Mukherjee, N.D. Rudd, A.V. Desai, J. Li, S.K. Ghosh, Chem. Soc. Rev. 46 (2017) 3242.
[391] J. Han, D. Wang, Y. Du, S. Xi, Z. Chen, S. Yin, T. Zhou, R. Xu, Appl. Catal. A Gen. 521 (2016) 83.
[392] C.-C. Wang, X.-D. Du, J. Li, X.-X. Guo, P. Wang, J. Zhang, Appl. Catal. B 193 (2016) 198.
[393] S. Mosleh, M.R. Rahimi, M. Ghaedi, K. Dashtian, S. Hajati, RSC Adv. 6 (2016) 17204.
[394] H. Chen, Z.-G. Gu, S. Mirza, S.-H. Zhang, J. Zhang, J. Mater. Chem. A 6 (2018) 7175.
[395] M.H. Xie, R. Shao, X.G. Xi, G.H. Hou, R.F. Guan, P.Y. Dong, Q.F. Zhang, X.L. Yang, Chem. Eur. J 23 (2017) 3931.
[396] R.M. van der Veen, O.-H. Kwon, A. Tissot, A. Hauser, A.H. Zewail, Nature Chemistry 5 (2013) 395.
[397] K. Healey, W.B. Liang, P.D. Southon, T.L. Church, D.M. D'Alessandro, J. Mater. Chem. A 4 (2016) 10816.
[398] L. Heinke, M. Cakici, M. Dommaschk, S. Grosjean, R. Herges, S. Braese, C. Woell, ACS Nano 8 (2014) 1463.
[399] H.Q. Li, M.R. Martinez, Z. Perry, H.C. Zhou, P. Falcaro, C. Doblin, S. Lim, A.J. Hill, B. Halstead, M.R. Hill, Chem.-Eur. J. 22 (2016) 11176.
[400] D.K. Maity, A. Dey, S. Ghosh, A. Halder, P.P. Ray, D. Ghoshal, Inorg. Chem. 57 (2018) 251.
[401] A.B. Kanj, K. Muller, L. Heinke, Macromol. Rapid Commun. 39 (2018).
[402] L.L. Gong, W.T. Yao, Z.Q. Liu, A.M. Zheng, J.Q. Li, X.F. Feng, L.F. Ma, C.S. Yan, M. B. Luo, F. Luo, J. Mater. Chem. A 5 (2017) 7961.
[403] H.A. Schwartz, S. Olthof, D. Schaniel, K. Meerholz, U. Ruschewitz, Inorg. Chem. 56 (2017) 13100.
[404] E. Caballero-Mancebo, B. Cohen, J.M. Moreno, A. Corma, U. Diaz, A. Douhal, ACS Omega 3 (2018) 1600.

[405] T.J. Reade, T.S. Murphy, J.A. Calladine, R. Horvath, I.P. Clark, G.M. Greetham, M. Towrie, W. Lewis, M.W. George, N.R. Champness, Philos. Trans. Royal Soc. Math. Phys. Eng. Sci. 375 (2017).
[406] Y. Wu, S. Henke, G. Kieslich, I. Schwedler, M. Yang, D.A.X. Fraser, D. O'Hare, Angew. Chem.-Int. Edit. 55 (2016) 14081.
[407] M. Mazaj, V. Kaucic, N.Z. Logar, Acta Chim. Slovenica 63 (2016) 440.
[408] M. Dell'Angela, T. Anniyev, M. Beye, R. Coffee, A. Foehlisch, J. Gladh, T. Katayama, S. Kaya, O. Krupin, J. LaRue, A. Mogelhoj, D. Nordlund, J.K. Norskov, H. Oberg, H. Ogasawara, H. Ostrom, L.G.M. Pettersson, W.F. Schlotter, J.A. Sellberg, F. Sorgenfrei, J.J. Turner, M. Wolf, W. Wurth, A. Nilsson, Science 339 (2013) 1302.
[409] Y. Obara, H. Ito, T. Ito, N. Kurahashi, S. Thurmer, H. Tanaka, T. Katayama, T. Togashi, S. Owada, Y. Yamamoto, S. Karashima, J. Nishitani, M. Yabashi, T. Suzuki, K. Misawa, Struct. Dyn. 4 (2017).
[410] M. Naumova, D. Khakhulin, M. Rebarz, M. Rohrmuller, B. Dicke, M. Biednov, A. Britz, S. Espinoza, B. Grimm-Lebsanft, M. Kloz, N. Kretzschmar, A. Neuba, J. Ortmeyer, R. Schoch, J. Andreasson, M. Bauer, C. Bressler, W.G. Schmidt, G. Henkel, M. Rubhausen, Phys. Chem. Chem. Phys. 20 (2018) 6274.
[411] S. Neppl, J. Mahl, A.S. Tremsin, B. Rude, R.M. Qiao, W.L. Yang, J.H. Guo, O. Gessner, Faraday Discuss 194 (2016) 659.
[412] G. Smolentsev, A. Guda, X.Y. Zhang, K. Haldrup, E.S. Andreiadis, M. Chayarot-Kerlidou, S.E. Canton, M. Nachtegaal, V. Artero, V. Sundstrom, J. Phys. Chem. C 117 (2013) 17367.
[413] L.J. Murray, M. Dinca, J.R. Long, Chem. Soc. Rev. 38 (2009) 1294.
[414] M.P. Suh, H.J. Park, T.K. Prasad, D.W. Lim, Chem. Rev. 112 (2012) 782.
[415] Y.B. He, W. Zhou, G.D. Qian, B.L. Chen, Chem. Soc. Rev. 43 (2014) 5657.
[416] T.M. McDonald, J.A. Mason, X.Q. Kong, E.D. Bloch, D. Gygi, A. Dani, V. Crocella, F. Giordanino, S.O. Odoh, W.S. Drisdell, B. Vlaisavljevich, A.L. Dzubak, R. Poloni, S.K. Schnell, N. Planas, K. Lee, T. Pascal, L.W.F. Wan, D. Prendergast, J.B. Neaton, B. Smit, J.B. Kortright, L. Gagliardi, S. Bordiga, J.A. Reimer, J.R. Long, Nature 519 (2015) 303.
[417] D.A. Reed, B.K. Keitz, J. Oktawiec, J.A. Mason, T. Runcevski, D.J. Xiao, L.E. Darago, V. Crocella, S. Bordiga, J.R. Long, Nature 550 (2017) 96.
[418] M. Du, L. Li, M.X. Li, R. Si, RSC Adv. 6 (2016) 62705.
[419] Y. Chen, H. Wang, J. Li, J.V. Lockard, J. Mater. Chem. A 3 (2015) 4945.
[420] H. Xue, Q.H. Chen, F.L. Jiang, D.Q. Yuan, G.X. Lv, L.F. Liang, L.Y. Liu, M.C. Hong, Chem. Sci. 7 (2016) 5983.
[421] J.Y. Zhang, N. Zhang, L.J. Zhang, Y.Z. Fang, W. Deng, M. Yu, Z.Q. Wang, L. Li, X.Y. Liu, J.Y. Li, Sci. Rep. 5 (2015) 10.
[422] Z.Q. Bai, L.Y. Yuan, L. Zhu, Z.R. Liu, S.Q. Chu, L.R. Zheng, J. Zhang, Z.F. Chai, W.Q. Shi, Introduction of amino groups into acid-resistant MOFs for enhanced U (VI) sorption, J. Mater. Chem. A (2015) 525.
[423] S.S.-Y. Chui, S.M.-F. Lo, J.P.H. Charmant, A.G. Orpen, I.D. Williams, Science 283 (1999) 1148.
[424] C. Prestipino, L. Regli, J.G. Vitillo, F. Bonino, A. Damin, C. Lamberti, A. Zecchina, P.L. Solari, K.O. Kongshaug, S. Bordiga, Chem. Mater. 18 (2006) 1337.
[425] S. Bordiga, L. Regli, F. Bonino, E. Groppo, C. Lamberti, B. Xiao, P.S. Wheatley, R. E. Morris, A. Zecchina, Phys. Chem. Chem. Phys. 9 (2007) 2676.
[426] K.-S. Lin, A.K. Adhikari, C.-N. Ku, C.-L. Chiang, H. Kuo, Int. J. Hydrog. Energy 37 (2012) 13865.
[427] W. Zhang, O. Kozachuk, R. Medishetty, A. Schneemann, R. Wagner, K. Khaletskaya, K. Epp, A. Fischer Roland, Eur. J. Inorg. Chem. 2015 (2015) 3913.
[428] H. Furukawa, Y.B. Go, N. Ko, Y.K. Park, F.J. Uribe-Romo, J. Kim, M. O'Keeffe, O. M. Yaghi, Inorg. Chem. 50 (2011) 9147.
[429] S. Marx, W. Kleist, A. Baiker, J. Catal. 281 (2011) 76.
[430] D. Sheberla, J.C. Bachman, J.S. Elias, C.-J. Sun, Y. Shao-Horn, M. Dincă, Nat. Mater. 16 (2016) 220.
[431] J. Shin, M. Kim, J. Cirera, S. Chen, G.J. Halder, T.A. Yersak, F. Paesani, S.M. Cohen, Y.S. Meng, J. Mater. Chem. A 3 (2015) 4738.
[432] Q. Pang, X. Liang, C.Y. Kwok, L.F. Nazar, J. Electrochem. Soc. 162 (2015) A2567.
[433] C. Li, X. Hu, W. Tong, W. Yan, X. Lou, M. Shen, B. Hu, ACS Appl. Mater. Interfaces 9 (2017) 29829.
[434] X. Meng, C. Wan, Y. Wang, X. Ju, J. Alloys Compounds 735 (2018) 1637.
[435] J. Singh, C. Lamberti, J.A. van Bokhoven, Chem. Soc. Rev. 39 (2010) 4754.
[436] A.M. Beale, S.D.M. Jacques, B.M. Weckhuysen, Chem. Soc. Rev. 39 (2010) 4656.
[437] A. Hornes, A.B. Hungria, P. Bera, A.L. Camara, M. Fernandez-Garcia, A. Martinez-Arias, L. Barrio, M. Estrella, G. Zhou, J.J. Fonseca, J.C. Hanson, J.A. Rodriguez, J. Am. Chem. Soc. 132 (2010) 34.
[438] C. Lamberti, S. Bordiga, F. Bonino, C. Prestipino, G. Berlier, L. Capello, F. D'Acapito, F. Xamena, A. Zecchina, Phys. Chem. Chem. Phys. 5 (2003) 4502.
[439] S.J. Tinnemans, J.G. Mesu, K. Kervinen, T. Visser, T.A. Nijhuis, A.M. Beale, D.E. Keller, A.M.J. van der Eerden, B.M. Weckhuysen, Catal. Today 113 (2006) 3.
[440] J.L. Fulton, J.C. Linehan, T. Autrey, M. Balasubramanian, Y. Chen, N.K. Szymczak, J. Am. Chem. Soc. 129 (2007) (1949) 11936.
[441] D. Gamarra, C. Belver, M. Fernandez-Garcia, A. Martinez-Arias, J. Am. Chem. Soc. 129 (2007) 12064.
[442] P.J. Ellis, I.J.S. Fairlamb, S.F.J. Hackett, K. Wilson, A.F. Lee, Angew. Chem., Int. Edit. 49 (2010) 1820.
[443] E. Groppo, W. Liu, O. Zavorotynska, G. Agostini, G. Spoto, S. Bordiga, C. Lamberti, A. Zecchina, Chem. Mater. 22 (2010) 2297.
[444] K. Fottinger, J.A. van Bokhoven, M. Nachtegaal, G. Rupprechter, J. Phys. Chem. Lett. 2 (2011) 428.
[445] K. Paredis, L.K. Ono, S. Mostafa, L. Li, Z.F. Zhang, J.C. Yang, L. Barrio, A.I. Frenkel, B.R. Cuenya, J. Am. Chem. Soc. 133 (2011) 6728.
[446] A.I. Frenkel, J.A. Rodriguez, J.G.G. Chen, ACS Catal. 2 (2012) 2269.
[447] V.F. Kispersky, A.J. Kropf, F.H. Ribeiro, J.T. Miller, Phys. Chem. Chem. Phys. 14 (2012) 2229.
[448] C. Barzan, D. Gianolio, E. Groppo, C. Lamberti, V. Monteil, E.A. Quadrelli, S. Bordiga, Chem. Eur. J. 19 (2013) 17277.
[449] T.V.W. Janssens, H. Falsig, L.F. Lundegaard, P.N.R. Vennestrom, S.B. Rasmussen, P.G. Moses, F. Giordanino, E. Borfecchia, K.A. Lomachenko, C. Lamberti, S. Bordiga, A. Godiksen, S. Mossin, P. Beato, ACS Catal. 5 (2015) 2832.
[450] M. Signorile, A. Damin, A. Budnyk, C. Lamberti, A. Puig-Molina, P. Beato, S. Bordiga, J. Catal. 328 (2015) 225.
[451] I. Lezcano-Gonzalez, R. Oord, M. Rovezzi, P. Glatzel, S.W. Botchway, B.M. Weckhuysen, A.M. Beale, Angew. Chem., Int. Edit. 55 (2016) 5215.
[452] A. Marberger, D. Ferri, M. Elsener, O. Krocher, Angew. Chem., Int. Edit. 55 (2016) (1994) 11989.
[453] A.M. Abdel-Mageed, G. Kucerova, J. Bansmann, R.J. Behm, ACS Catal. 7 (2017) 6471.
[454] M. Manzoli, F. Vindigni, T. Tabakova, C. Lamberti, D. Dimitrov, K. Ivanov, G. Agostini, J. Mater. Chem. A 5 (2017) 2083.
[455] A. Martini, E. Borfecchia, K.A. Lomachenko, I.A. Pankin, C. Negri, G. Berlier, P. Beato, H. Falsig, S. Bordiga, C. Lamberti, Chem. Sci. 8 (2017) 6836.
[456] H. Matsui, N. Ishiguro, T. Uruga, O. Sekizawa, K. Higashi, N. Maejima, M. Tada, Angew. Chem., Int. Edit. 56 (2017) 9371.
[457] M.J. Munoz-Batista, D.M. Meira, G. Colon, A. Kubacka, M. Fernandez-Garcia, Angew. Chem., Int. Edit. 57 (2018) 1199.
[458] A.M. Beale, A.M.J. van der Eerden, K. Kervinen, M.A. Newton, B.M. Weckhuysen, Chem. Commun. (2005) 3015.
[459] M.A. Newton, A.J. Dent, S.G. Fiddy, B. Jyoti, J. Evans, Catal. Today 126 (2007) 64.
[460] G. Agostini, C. Lamberti, L. Palin, M. Milanesio, N. Danilina, B. Xu, M. Janousch, J.A. van Bokhoven, J. Am. Chem. Soc. 132 (2010) 667.
[461] G. Agostini, C. Lamberti, R. Pellegrini, G. Leofanti, F. Giannici, A. Longo, E. Groppo, ACS Catal. 4 (2014) 187.
[462] E. Groppo, G. Agostini, E. Borfecchia, A. Lazzarini, W. Liu, C. Lamberti, F. Giannici, G. Portale, A. Longo, ChemCatChem 7 (2015) 2188.
[463] Y. Li, D. Zakharov, S. Zhao, R. Tappero, U. Jung, A. Elsen, P. Baumann, R.G. Nuzzo, E.A. Stach, A.I. Frenkel, Nat. Commun. 6 (2015) 6.
[464] M.A. Newton, Catalysts 7 (2017) 58.
[465] P. Glatzel, U. Bergmann, Coord. Chem. Rev. 249 (2005) 65.
[466] O.V. Safonova, M. Tromp, J.A. van Bokhoven, F.M.F. de Groot, J. Evans, P. Glatzel, J. Phys. Chem. B 110 (2006) 16162.
[467] P. Glatzel, M. Sikora, G. Smolentsev, M. Fernandez-Garcia, Catal. Today 145 (2009) 294.
[468] A. Iglesias-Juez, A.M. Beale, K. Maaijen, T.C. Weng, P. Glatzel, B.M. Weckhuysen, J. Catal. 276 (2010) 268.
[469] L.R. Merte, F. Behafarid, D.J. Miller, D. Friebel, S. Cho, F. Mbuga, D. Sokaras, R. Alonso-Mori, T.C. Weng, D. Nordlund, A. Nilsson, B.R. Cuenya, ACS Catal. 2 (2012) 2371.
[470] M. Bauer, Phys. Chem. Chem. Phys. 16 (2014) 13827.
[471] A. Boubnov, H.W.P. Carvalho, D.E. Doronkin, T. Gunter, E. Gallo, A.J. Atkins, C. R. Jacob, J.D. Grunwaldt, J. Am. Chem. Soc. 136 (2014) 13006.
[472] A. Gorczyca, V. Moizan, C. Chizallet, O. Proux, W. Del Net, E. Lahera, J.L. Hazemann, P. Raybaud, Y. Joly, Angew. Chem., Int. Edit. 53 (2014) 12426.
[473] A.P. Hitchcock, M.F. Toney, J. Synchrotron Radiat. 21 (2014) 1019.
[474] F. Giordanino, E. Borfecchia, K.A. Lomachenko, A. Lazzarini, G. Agostini, E. Gallo, A.V. Soldatov, P. Beato, S. Bordiga, C. Lamberti, J. Phys. Chem. Lett. 5 (2014) 1552.
[475] D. Friebel, M.W. Louie, M. Bajdich, K.E. Sanwald, Y. Cai, A.M. Wise, M.J. Cheng, D. Sokaras, T.C. Weng, R. Alonso-Mori, R.C. Davis, J.R. Bargar, J.K. Norskov, A. Nilsson, A.T. Bell, J. Am. Chem. Soc 137 (2015) 1305.
[476] S.M. Butorin, K.O. Kvashnina, J.R. Vegelius, D. Meyer, D.K. Shuh, Proc. Natl. Acad. Sci. USA 113 (2016) 8093.
[477] M. Babucci, C.Y. Fang, A.S. Hoffman, S.R. Bare, B.C. Gates, A. Uzun, ACS Catal. 7 (2017) 6969.
[478] R.G. Castillo, R. Banerjee, C.J. Allpress, G.T. Rohde, E. Bill, L. Que, J.D. Lipscomb, S. DeBeer, J. Am. Chem. Soc 139 (2017) 18024.
[479] O. Hirsch, K. Kvashnina, C. Willa, D. Koziej, Chem. Mater. 29 (2017) 1461.
[480] O.V. Safonova, M. Florea, J. Bilde, P. Delichere, J.M.M. Millet, J. Catal. 268 (2009) 156.
[481] N. Lee, T. Petrenko, U. Bergmann, F. Neese, S. DeBeer, J. Am. Chem. Soc. 132 (2010) 9715.
[482] J.C. Swarbrick, Y. Kvashnin, K. Schulte, K. Seenivasan, C. Lamberti, P. Glatzel, Inorg. Chem. 49 (2010) 8323.
[483] E. Gallo, C. Lamberti, P. Glatzel, Phys. Chem. Chem. Phys. 13 (2011) 19409.
[484] K.M. Lancaster, M. Roemelt, P. Ettenhuber, Y.L. Hu, M.W. Ribbe, F. Neese, U. Bergmann, S. DeBeer, Science 334 (2011) 974.
[485] L. Mino, V. Colombo, J.G. Vitillo, C. Lamberti, S. Bordiga, E. Gallo, P. Glatzel, A. Maspero, S. Galli, Dalton Trans. 41 (2012) 4012.
[486] E. Gallo, F. Bonino, J.C. Swarbrick, T. Petrenko, A. Piovano, S. Bordiga, D. Gianolio, E. Groppo, F. Neese, C. Lamberti, P. Glatzel, ChemPhysChem 14 (2013) 79.
[487] K.A. Lomachenko, C. Garino, E. Gallo, D. Gianolio, R. Gobetto, P. Glatzel, N. Smolentsev, G. Smolentsev, A.V. Soldatov, C. Lamberti, L. Salassa, Phys. Chem. Chem. Phys. 15 (2013) 16152.
[488] C.J. Pollock, K. Grubel, P.L. Holland, S. DeBeer, J. Am. Chem. Soc. 135 (2013) (1808) 11803.
[489] K. Seenivasan, E. Gallo, A. Piovano, J.G. Vitillo, A. Sommazzi, S. Bordiga, C. Lamberti, P. Glatzel, E. Groppo, Dalton Trans. 42 (2013) 12706.

[490] E. Gallo, P. Glatzel, Adv. Mater. 26 (2014) 7730.
[491] E. Gallo, A. Piovano, C. Marini, O. Mathon, S. Pascarelli, P. Glatzel, C. Lamberti, G. Berlier, J. Phys. Chem. C 118 (2014) 11745.
[492] E. Groppo, E. Gallo, K. Seenivasan, K.A. Lomachenko, A. Sommazzi, S. Bordiga, P. Glatzel, R. van Silfhout, A. Kachatkou, W. Bras, C. Lamberti, ChemCatChem 7 (2015) 1432.
[493] C.J. Pollock, S. DeBeer, Acc. Chem. Res. 48 (2015) 2967.
[494] G. Vanko, A. Bordage, M. Papai, K. Haldrup, P. Glatzel, A.M. March, G. Doumy, A. Britz, A. Galler, T. Assefa, D. Cabaret, A. Juhin, T.B. van Driel, K.S. Kjaer, A. Dohn, K.B. Moller, H.T. Lemke, E. Gallo, M. Rovezzi, Z. Nemeth, E. Rozsalyi, T. Rozgonyi, J. Uhlig, V. Sundstrom, M.M. Nielsen, L. Young, S.H. Southworth, C. Bressler, W. Gawelda, J. Phys. Chem. C 119 (2015) 5888.
[495] R. Kopelent, J.A. van Bokhoven, M. Nachtegaal, J. Szlachetko, O.V. Safonova, Phys. Chem. Chem. Phys. 18 (2016) 32486.
[496] S.C. Jensen, K.M. Davis, B. Sullivan, D.A. Hartzler, G.T. Seidler, D.M. Casa, E. Kasman, H.E. Colmer, A.A. Massie, T.A. Jackson, Y. Pushkar, J. Phys. Chem. Lett. 8 (2017) 2584.
[497] R.Q. Zhang, H. Li, J.S. McEwen, J. Phys. Chem. C 121 (2017) 25759.
[498] T. Kroll, C. Weninger, R. Alonso-Mori, D. Sokaras, D.L. Zhu, L. Mercadier, V.P. Majety, A. Marinelli, A. Lutman, M.W. Guetg, F.J. Decker, S. Boutet, A. Aquila, J. Koglin, J. Koralek, D.P. DePonte, J. Kern, F.D. Fuller, E. Pastor, T. Fransson, Y. Zhang, J. Yano, V.K. Yachandra, N. Rohringer, U. Bergmann, Phys. Rev. Lett. 120 (2018) 133203.
[499] M. Altarelli, Nucl. Instrum. Methods Phys. Res. Sect. B-Beam Interact. Mater. Atoms 269 (2011) 2845.
[500] M. Altarelli, A.P. Mancuso, Philos. Trans. R. Soc. B-Biol. Sci. 369 (2014) 20130311.
[501] U. Bergman, V.K. Yachandra, J. Yano, X-Ray Free Electron Lasers: Applications in Materials, Chemistry and Biology, Royal Society of Chemistry, 2017.
[502] M. Cotte, E. Pouyet, M. Salome, C. Rivard, W. De Nolf, H. Castillo-Michel, T. Fabris, L. Monico, K. Janssens, T. Wang, P. Sciau, L. Verger, L. Cormier, O. Dargaud, E. Brun, D. Bugnazet, B. Fayard, B. Hesse, A.E.P. Del Real, G. Veronesi, J. Langlois, N. Balcar, Y. Vandenberghe, V.A. Sole, J. Kieffer, R. Barrett, C. Cohen, C. Cornu, R. Baker, E. Gagliardini, E. Papillon, J. Susini, J. Anal. Atomic Spectrom. 32 (2017) 477.